1972

# Measurement of low frequency noise in mos structures with 20-40 thick oxides

Vikram Kumar
*Lehigh University*

# MEASUREMENT OF LOW FREQUENCY NOISE IN MOS STRUCTURES WITH 20-40 Å THICK OXIDES

Vikram Kumar

## ABSTRACT

Since McWhorter [6] suggested that flicker noise is related to surface states in semiconductor devices, several attempts have been made to establish this relationship using MOS transistors and other devices. However, since the surface state density distribution of such devices cannot be measured, the correlation has been only qualitatively established by Sah and Hielscher [7] and others [8,9]. Recently Kar and Dahlke [21,22] have developed MOS structures with 20 - 40 Å thick oxide layers that allow measuring the interface state density and the noise simultaneously and independently. In this thesis, a measuring technique is developed to determine the low frequency noise of such MOS structures. Measurements of three samples show the suitability of the experimental technique and its reproducibility, revealing a close relationship between the low frequency noise and the energy distribution of surface states. A theoretical model is proposed that explains the experimental results; a further study of low frequency noise and surface states of the MOS diodes is expected to establish the relationship in detail.

# MEASUREMENT OF LOW FREQUENCY NOISE IN MOS STRUCTURES WITH 20 - 40 Å THICK OXIDES

by

Vikram Kumar

A Thesis

Presented to the Graduate Committee

of Lehigh University

in candidacy for the Degree of

Master of Science

in

Electrical Engineering

Lehigh University

1972

CERTIFICATE OF APPROVAL

This thesis is accepted in partial fulfilment of the requirements for the degree of Master of Science.

Dec. 13. 1971

Date

Professor in Charge

Alfred K. Susskind

Head of the Department of
Electrical Engineering

ACKNOWLEDGEMENTS

The author expresses deepest gratitude to Prof. W. E. Dahlke without whose patient guidance and encouragement this work would not have been possible. He is grateful to Prof. J. G. Ondria for his valuable time and help in developing the measuring system. He wishes to thank Dr. S. M. Sze of Bell Telephone Laboratories for providing samples.

The author appreciates the financial assistance from National Science Foundation supporting this work.

TABLE OF CONTENTS

## LIST OF FIGURES

ABSTRACT

Since McWhorter [6] suggested that flicker noise is related to surface states in semiconductor devices, several attempts have been made to establish this relationship using MOS transistors and other devices. However, since the surface state density distribution of such devices cannot be measured, the correlation has been only qualitatively established by Sah and Hielscher [7] and others [8,9]. Recently Kar and Dahlke [21,22] have developed MOS structures with 20 - 40 Å thick oxide layers that allow measuring the interface state density and the noise simultaneously and independently. In this thesis, a measuring technique is developed to determine the low frequency noise of such MOS structures. Measurements of three samples show the suitability of the experimental technique and its reproducibility, revealing a close relationship between the low frequency noise and the energy distribution of surface states. A theoretical model is proposed that explains the experimental results; a further study of low frequency noise and surface states of the MOS diodes is expected to establish the relationship in detail.

## 1. INTRODUCTION

Noise of electronic devices has been studied extensively because it limits the ultimate sensitivity of electronic systems. It sometimes also reveals details of physical device processes that are not measurable otherwise. All resistive devices show thermal noise which is frequency independent and well understood. Further; the devices exhibit a frequency dependent noise at low frequencies that can be classified in two types: (i) generation - recombination noise with a $1/(1 + \omega^2\tau^2)$ frequency dependence and a single time constant $\tau$, and (ii) flicker noise with 1/f frequency dependence and a distribution of time constants [1].

The first is due to generation - recombination of carriers in semiconductors and has been studied in junction field effect transistors (JFETs) by Sah [2] and Lauritzen [3], and in metal - oxide - silicon field effect transistors (MOSFETs) by Wu [4] and Yau and Sah [5]. This type of noise is well understood, and agreement between theory and experiment has been established for both JFETs [3] and MOSFETs [5].

The origin of flicker noise is not completely clear. It has been generally recognised [1] that spectra of the type $1/(1 + \omega^2\tau^2)$ when superimposed with a suitable time constant dispersion can yield a 1/f noise spectrum over a wide frequency range. The basic problem is to establish the mechanism that causes the time constant distribution. McWhorter [6] has attributed the distribution to electronic states in the oxide layer that are called surface states and exist

on all semiconductor surfaces. These states in the oxide layer communicate with the semiconductor bands by tunneling of carriers through the oxide, a process causing the necessary time constant distribution.

MOS transistors have been widely studied to show the relationship between low frequency noise and surface states. Sah and Hielscher [7], Abowitz et. al. [8], and Hsu et. al. [9] have shown experimentally that low frequency noise and surface states in MOS transistors are correlated; however, in each case the correlation was only indirectly and qualitatively substantiated. In recent years several theoretical models have been proposed for flicker noise in MOS transistor, [10-14]; most of them [12-14] are based on McWhorter's tunneling model [6]. Extensive experimental investigations [13,15-17] show that the flicker noise in this device is very complex, and theory and experiments do not agree in all respects. A detailed comparison of the theoretical models with the experimentally observed behavior requires an exact knowledge of the trap distribution across the energy gap and the oxide thickness. This information is usually not available since the surface state density under the gate of a MOS transistor cannot be measured easily.

Recently, gate controlled p-n junction diodes have been employed to study flicker noise [9,18,19]. Unlike the MOS transistor with its always inverted surface, this structure allows scanning of the Fermi level across the entire forbidden band gap. However, in this case also, the correlation of 1/f noise and surface states has been only indirectly and qualitatively established [19].

Nicollian and Melchior [20] proposed a theory of low

frequency noise in MOS diodes with thick oxide layers. They used a model that has been widely employed for studying Si-$SiO_2$ interface properties. However, this structure is not suitable for noise measurements since its conductance is extremely low ($10^{-8}$ mho and less). Recently Kar and Dahlke [21,22] have measured the surface state density of MOS diodes with 20 - 40 Å thick oxide layers. It is possible to measure simultaneously and independently the surface and noise properties of these diodes.

A theoretical model for low frequency noise of MOS diodes with a thin oxide layer is given in Section 2. The main purpose of this thesis is to show the feasibility of the noise measurements. Since the admittance of the test diodes is low (between $10^{-8}$ and $10^{-3}$ mhos depending on bias and frequency), the conventional noise mesurement method [23] had to be modified. The employed technique is described in Section 3. Low frequency noise measurements of three samples are reported and discussed in Section 4. Conclusions are given in Section 5.

# 2. THEORY OF LOW FREQUENCY NOISE

## 2.1 Spectral Density of Device Noise

In this section a theoretical model is proposed to explain the low frequency noise of the employed MOS diodes with 20 - 40 Å thick oxide layers. The most important component of current through the test diode is due to majority carriers being emitted over the silicon barrier and then tunneling through the oxide barrier into the metal [21]. This thermionic emission current showing full shot noise noise [23] is derived similarly to that of an ideal Schottky barrier diode [24],

$$I_{em} = A^{*}T^{2}\, e^{-(q\Phi/kT)}(e^{(qV_B/kT)} - 1) \,, \qquad (2.1)$$

where $A^{*}$ is Richardson's coefficient modified by tunneling of carriers through the oxide, $V_B$ is the applied bias, and $\Phi$ is the metal barrier height; cf. Fig. 1. Here, only the contribution to device noise from fluctuations of the surface state occupancy will be considered. These fluctuations are a consequence of generation - recombination of carriers in the surface states and result in a modulation of the barrier height. According to eq. (2.1), a fluctuation $\delta\Phi$ of the barrier height $\Phi$, induces a fluctuation of the current

$$\delta I_{em} = -I_{em}(q/kT)\,\delta\Phi \,. \qquad (2.2)$$

The barrier height for a n-type semiconductor [21],

$$\Phi = \Phi_m - \chi_m - (Q_{ss} + Q_{sc})/C_{ox} \,, \qquad (2.3)$$

depends on the surface state charge,

$$Q_{ss} = - qN_t \,, \qquad (2.4)$$

where the space charge $Q_{sc}$, the oxide capacitance $C_{ox}$, and the number

of occupied surface states $N_t$ ($cm^{-2}$) which are assumed to be of acceptor type.

For single energy level states at the interface with a generation - recombination time constant $\tau_R$, the spectral fluctuation density of the surface state occupancy is [23],

$$S_{\delta N_t} = 4N_T f_s(1-f_s)\,\tau_R/(1+\omega^2\tau_R^2) \quad , \tag{2.5}$$

where $N_T$ ($cm^{-2}$) is the total number of surface states, and $f_s$ ($= N_t/N_T$) the surface state occupancy factor. Combining equations (2.2) to (2.5), the spectral fluctuation density of the thermionic emission current is

$$S_{\delta I_{em}} = \frac{I_{em}^2\, q^4}{C_{ox}^2 k^2 T^2}\; 4N_T f_s(1-f_s)\,\tau_R/(1+\omega^2\tau_R^2) \quad . \tag{2.6}$$

A proposed equivalent circuit of the MOS diode [21] is shown in Fig. 2. For a single level surface state with a time constant $\tau_R$ [25], we have the relations,

$$G_p(\omega) = \frac{\omega^2\tau_R C_s}{1+\omega^2\tau_R^2} \quad , \quad C_p(\omega) = \frac{C_s}{1+\omega^2\tau_R^2} \quad , \quad C_s = \frac{q^2}{kT} N_T f_s(1-f_s) \quad . \tag{2.7}$$

Comparison of equations (2.6) and (2.7) yields

$$S_{\delta I_{em}} = 4kT\,(I_{em} q/C_{ox} kT)^2\; G_p(\omega)/\omega^2 \quad . \tag{2.8}$$

Thus, the diode will show 1/f noise if $G_p(\omega) \sim \omega$. The conductance, $G_p(\omega)$, contains implicitly as parameters the energy and space distributions of the surface states and their capture cross-section, $\sigma$.

## 2.2 Theoretical Models

Three different models for $\sigma$ will be considered:

(1) Nicollian and Melchior [20] assumed a constant capture cross-section, $\sigma$. This leads to eq. (2.7) for single energy level

states. The dotted lines in Fig. 3 illustrate a numerical example for the functions $G_p(\omega)$, $G_p(\omega)/\omega$, $G_p(\omega)/\omega^2 \sim i^2$, and $C_p(\omega)$. This model agrees well with measured $G_p(\omega)/\omega$ curves; however, it cannot explain the large frequency range of the experimental 1/f noise.

(2) McWhorter assumed tunneling of carriers into states lying in the oxide; their capture cross-section decreases exponentially with the oxide depth,

$$\sigma = \sigma_o e^{-\alpha x} , \quad \tau_R = \tau_o e^{\alpha x} . \tag{2.9}$$

For a state density $N'_T$ ($cm^{-2}$), constant between $x_1$ and $x_2$ of the oxide, the relations,

$$G_p(\omega) = \frac{C'_s}{2\ln(\tau_2/\tau_1)} ,$$

$$C_p(\omega) = C'_s \left(1 - \frac{\ln(\omega\tau_2)}{\ln(\tau_2/\tau_1)}\right) , \tag{2.10}$$

$$C'_s = (q^2/kT)\, N'_T f_s (1-f_s) ,$$

in the frequency range, $\omega\tau_1 << 1 << \omega\tau_2$, where $\tau_1 = \tau_R(x_1)$ and $\tau_2 = \tau_R(x_2)$; cf. eq. (2.9). Numerical values of $G_p(\omega)$, $G_p(\omega)/\omega$, $G_p(\omega)/\omega^2$, and $C_p(\omega)$ calculated from eq. (2.10) are presented as dashed curves in Fig. 3. The current fluctuation $i^2 \sim G_p(\omega)/\omega^2$ shows an extremely broad 1/f range; however, this model fails to explain the measured $G_p(\omega)/\omega$ maxima, as discussed by Nicollian and Goetzberger [25].

(3) The $\sigma$-distributions of models (1) and (2) are unrealistic. The true distribution must reflect the lattice structure of the oxide, as indicated by the dashed lines of Fig. 4. It should have a broad maximum at the interface layer, k=0, in contrast to the pointed line for model (2), and then smooth out by averaging the

tunneling effect deeper in the oxide. The full line in Fig. 4 presents as reasonable approximation of the $\delta$-distribution; consequently, the functions $G_p(\omega)$, $G_p(\omega)/\omega$, $G_p(\omega)/\omega^2$, and $C_p(\omega)$ drawn as full lines for model (3), are linear superpositions of the corrospcnding curves for models (1) and (2). The bump in the noise curve $G_p(\omega)/\omega^2$ in Fig. 3 is caused by states in the interface layer and the 1/f range by states in the oxide.

The theoretical curves for the realistic model (3) will be compared with observed results in Section 4.

## 3. NOISE MEASUREMENTS

The technique used here for measuring the low frequency noise of MOS diodes with 20 - 40 Å thick oxide layers is a modification of a well known method [23, page 57], that is necessary because the test diode has a very low and frequency and bias dependent admittance. Its conductance usually varies between $10^{-8}$ mho and $10^{-3}$ mho and the capacitance between 5 pF and 400 pF. Since the impedance of the reverse or moderately forward biased diode can be as high as $10^{8}$ ohms, true ac and dc current sources are difficult to obtain. The solution of this problem is discussed in Section 3.1, and the noise measurement technique is described in Section 3.2.

### 3.1 Measuring System

A block diagram of the experimental set-up is shown in Fig. 5. The different instruments and their functions are described in this paragraph.

A variable dc voltage supply is used to bias the test device. $R_b$ is a large resistor of which the exact value needs not to be known. Values of $R_b$ = 1000 Mohm, 10 Mohm, and 300 kohm are chosen so that they are at least 100 times greater than the device impedance and that they allow the required biasing current to be drawn from the battery. A Keithley Electrometer 610B is used to measure the bias current; after that, it is replaced by a short circuit to prevent any contribution of its noise to the measuring system. The test diode is enclosed in a shielded, light-tight box. The admittance, $Y_s$, is a parallel combination of a resistor $R_s$ and a capacitor $C_s$ chosen carefully to simulate the diode admittance at operating bias

and measurement frequency. Details of the combination are described in Appendix E. The thermal noise generated by the simulated admittance, $Y_s$, is compared with the device noise.

The noise voltage of the test device is amplified by the low noise amplifier PAR 113, which is described in AppendixD. The output of the amplifier is displayed on an oscilloscope to confirm that it is not saturated. It is measured with one of the two available wave analyzers. The Quantech Lab 303 wave analyzer reads voltages in the range of 0.1 mV to 300 V rms and allows to select a bandwidth of 10 Hz, 30 Hz, 100 Hz or 1000 Hz. Choosing the indicated bandwidth of 10 Hz in the frequency range of 20 Hz to 80 kHz, a corrosponding effective noise bandwidth of 8.8 ± 0.5 Hz was determined (cf. Appendix B). The Hewlett Packard 302 AR wave analyzer reading voltages in the range of 30 V to 300 V rms has a fixed signal bandwidth of 2 Hz between 5 Hz and 50 kHz frequency; its effective noise bandwidth is 2.05 ± 0.1 Hz. The recorder output of the wave analyzer is fed through a time averaging circuit of 2.5 seconds time constant into an X-Y recorder.

The available noise power of the diode is compared with the available signal power of a Heathkit IG-18 signal generator at each measuring frequency. The exactly known impedance, Z, chosen at least thousand times larger than the device impedance, converts the signal voltage source into an ac current source. For a reverse or moderately forward biased diode, Z is represented by a capacitance of 0.95 pF, and for a larger forward bias or lower device impedance, by a resistor of 5 Mohm. A frequency counter determines the exact measuring frequency.

## 3.2 Measuring Technique

In principle, the device noise can be represented either by a short circuit current or by an open circuit voltage. Both representations are equally useful for a purely resistive device; however, for our test device consisting of a resistor shunted by a capacitor the open circuit voltage is frequency dependent. In our case the current source representation is superior since it is independent of capacitance and hence of frequency. Therefore, the device noise is represented by an equivalent noise conductance, $G_{eq}$, generating the same short circuit thermal noise current as the device at room temperature. The quantity directly measured is the "total short circuit input noise current", $i_{tot}$, additionally applied to the amplifier input to double the output noise power. $i_{tot}$ includes noise contributions from the test device, the amplifier and other noise sources in the measuring system.

### 3.21 The Total Short Circuit Input Noise Current

The basic set-up for measuring $i_{tot}$ is shown in Fig. 6a. First, the amplifier output voltage $V_n$, originating from contributions of the noise source and the amplifier, is noted for $I_s = 0$, as indicated in Fig. 6b. The available input noise power of the set-up is by definition,

$$N_{in} = \frac{\overline{|i_{tot}|^2}}{4\ \mathrm{Re}(Y_s)} = \frac{\overline{|i|^2}}{4\ \mathrm{Re}(Y_s)} + kT(F-1)B\,, \qquad (3.1)$$

$\overline{|i|^2}$ the mean square value of the short circuit noise current, T the measurement temperature, F the amplifier noise factor, cf. Appendix C, and B the effective noise bandwidth of the measuring system,

cf. Appendix **B**. Second, the current $I_s$ is adjusted so that the amplifier output voltage increases to $NV_n$. The corrosponding available power of the signal source is

$$\frac{I_s^2}{4\,\mathrm{Re}(Y_s)} = (N^2 - 1)N_{in} = (N^2 - 1)\,\frac{\overline{|i_{tot}|^2}}{4\,\mathrm{Re}(Y_s)}\ , \tag{3.2}$$

hence

$$\overline{|i_{tot}|^2} = I_s^2/(N^2 - 1)\ . \tag{3.3}$$

If $N^2 = 2$,

$$\overline{|i_{tot}|^2} = I_s^2\ , \tag{3.3a}$$

and if $N^2 \gg 1$,

$$\overline{|i_{tot}|^2} = (I_s/N)^2\ . \tag{3.3b}$$

In practice the current source $I_s$ is obtained by using the impedance, Z, in series with a voltage source, $V_s$. Choosing the impedance large compared with the device impedance, $|Z| \gg |1/Y_s|$, yields

$$I_s = V_s/|Z|\ , \tag{3.4}$$

and combining eqs. (3.3) and (3.4),

$$\overline{|i_{tot}|^2} = V_s^2/(N^2 - 1)|Z|^2\ . \tag{3.5}$$

Defining the signal current,

$$I_{tot} \equiv \frac{V_s}{(N^2 - 1)^{1/2}|Z|} = \left(\overline{|i_{tot}|^2}\right)^{1/2}, \tag{3.6}$$

for $N^2 \gg 1$,

$$I_{tot} = V_s/N|Z| \tag{3.6a}$$

is found. The quantity $I_{tot}$ contains contributions from the amplifier noise and the unknown noise source; therefore, the next step is to extract the contribution of the noise source.

### 3.22 Device Noise

To measure the device noise, the test diode is placed in the position of the noise source in Fig. 6, and the rms value of the total noise current with diode, $I_{tot,D}$, is determined as explained in Section 3.21. Next, the diode is replaced by the simulating admittance, $Y_s$, and the rms total noise current, $I_{tot,Y}$, determined. Defining the conductances $G_D$ and $G_Y$ by

$$I^2_{tot,D} = 4kTG_DB \ , \tag{3.7a}$$

$$I^2_{tot,Y} = 4kTG_YB \ , \tag{3.7b}$$

from eqs. (3.1), (3.6) and (3.7), the relations

$$\frac{4\ kTG_DB}{4\ Re(Y_s)} = \frac{4kTG_{eq}B}{4\ Re(Y_s)} + kT(F-1)B \ , \tag{3.8a}$$

$$\frac{4\ kTG_YB}{4\ Re(Y_s)} = \frac{4kTRe(Y_s)B}{4\ Re(Y_s)} + kT(F-1)B \ , \tag{3.8b}$$

$$G_{eq} = G_D - G_Y + G_s \ , \tag{3.9}$$

are obtained. $G_{eq}$ is the equivalent noise conductance of the test diode, and $G_s = Re(Y_s)$. Often $G_Y$ and $G_s$ are negligible compared with $G_D$, then

$$G_{eq} = G_D \ . \tag{3.9a}$$

To find $G_{eq}$ according to eq.(3.9), the effective noise bandwidth, B, is determined according to Appendix **B**.

### 3.3 Accuracy of Measurements

The accuracy of the measuring technique is estimated by employing the standard formula [26] for the probable error of

$U = U(u_1, u_2)$,

$$\Delta U = [(\partial U/\partial u_1)\Delta u_1]^2 + [(\partial U/\partial u_2)\Delta u_2]^{2\ 1/2}. \qquad (3.10)$$

$\Delta u_1$ and $\Delta u_2$ are the probable errors in the parameters $u_1$ and $u_2$ respectively.

The measuring error of the signal voltage $V_s$ was 3%, of the impedance Z less than 1%, and neglegible for all other quantities. Denoting the probable errors of $I_{tot}$, $V_s$, Z, and N by $\Delta I_{tot}$, $\Delta V_s$, $\Delta Z$, and $\Delta N$, and using eqs. (3.6a) and (3.10), yields the probable error of $I_{tot}$,

$$\Delta I_{tot}/I_{tot} = [(\Delta V_s/V_s)^2 + (\Delta Z/Z)^2 + (\Delta N/N)^2]^{1/2} \approx 3\% . \qquad (3.11)$$

The probable error of the effective noise bandwidth, cf. eq. (B.2) of Appendix B, is

$$\Delta B/B = 2\,\Delta I_{tot}/I_{tot} \approx 6\% , \qquad (3.12)$$

of conductance $G_D$, cf. eq. (3.7),

$$\Delta G_D/G_D = [(2\,\Delta I_{tot}/I_{tot})^2 + (\Delta B/B)^2]^{1/2}$$
$$= [8(\Delta I_{tot}/I_{tot})^2]^{1/2} \approx 8.5\% , \qquad (3.13)$$

and of $G_Y$ also,

$$\Delta G_Y/G_Y = 8.5\% . \qquad (3.13a)$$

The probable error of $G_{eq}$ calculated from eq. (3.9) is

$$\Delta G_{eq} = [(\Delta G_D)^2 + (\Delta G_Y)^2]^{1/2}$$
$$= 0.085\ [G_D^{\ 2} + G_Y^{\ 2}]^{1/2} . \qquad (3.14)$$

This equation simplifies if $G_D \gg G_Y$, which holds for most of the reported data,

$$\Delta G_{eq} = 0.085\ G_D = 0.085\ G_{eq}, \qquad (3.14a)$$

otherwise the probable error is larger.

In general, the measuring technique allowed determination of the equivalent noise conductance of the test diode, $G_{eq}$, with less than 10% error between 5 Hz and 50 kHz.

## 4. RESULTS AND DISCUSSION

The low frequency noise of three MOS samples, cf. Fig. 2, has been measured. They consisted of 1 ohm-cm n-type silicon with a thermally grown oxide layer of approximately 20 Å. The contact metal were 200 Å thick chromium reinforced by gold, the contact area $10^{-4}$ $cm^2$. These samples mounted in V-2 packages were kindly supplied by Bell Laboratories at Murray Hill, New Jersey.

First, the signal properties of the devices were measured. The current vs. voltage (I - V) characteristic was measured using the set-up shown in Fig. 7, and the admittance as function of frequency and bias in the measuring set-up of Fig. 8. The measured I - V characteristic of sample 1 is plotted in Fig. 9, the measured conductance vs. bias (G - V) curves with frequency as parameter in Fig. 10, and the measured capacitance vs. bias with frequency as parameter in Fig. 11. The device is in deep depletion for a bias $V_B < -0.7$ V. Accumulation was not reached since the device conductance increased beyond the measuring range of the capacitance bridge; therefore, oxide capacitance and surface state density of the sample could only be roughly estimated. The conductance curves show a large dispersion indicating surface states [21], between $V_B$ = -0.7 V and 0.0 V.

Figure 12 presents the measured equivalent noise conductance, $G_{eq}$, as function of frequency with bias as parameter. The conductance, $G_{eq}$, shows a $(1/f)^{\alpha}$ dependence at frequencies less than 200 Hz with $1.1 \lesssim \alpha \lesssim 1.3$, humps at a frequency of about 5 kHz, and a faster decrease at higher frequencies. This behavior of $G_{eq}$ resembles the full drawn curve, $G_p(\omega)/\omega^2$, of Fig. 3b. The

conductance, $G_{eq}$, of sample 1 is shown in Fig. 13 as function of the bias current, I, and the bias voltage, $V_B$, in reverse and forward directions. It shows $I^{\beta}$-dependence with $\beta \lesssim 2$ and bumps at the same reverse bias, $-0.7\ V \lesssim V_B \lesssim 0.0\ V$, at which the conductance maxima in Fig. 10 occur. This behavior is predicted by eq. (2.8) and shows the close relationship of low frequency noise and surface states.

The dispersion of the conductance vs. bias (G - V) curves of sample 2 in Fig. 14 is caused by surface states in the bias range of -0.8 V to 0.0 V. The $G_{eq}(f)$ curves for reverse bias in Fig. 15 resemble the full drawn theoretical $G_p(\omega)/\omega^2$ curve of Fig. 3b. The $G_{eq}(I)$ curves in Fig. 16 show only the interface state related bump in the reverse bias range covered by measurements.

Sample 3 in Fig. 17 shows a lower reverse saturation current than sample 1 in Fig. 9. The conductance curves in Fig. 18 exhibit frequency dependent maxima at reverse bias, $V_B$ = -0.7 V to -0.1 V. The $G_{eq}(f)$ curves in Fig. 19 are similar to that of the theoretical model (3) of Section 2.2. The $G_{eq}(I)$ curves in Fig. 20 increase approximately with the square of current and have bumps at the same bias $-0.7\ V \lesssim V_B \lesssim -0.1\ V$ as the conductance maxima in Fig. 18.

Figure 21 illustrates the ac conductance, $G_{ac} \equiv G - G_{dc}$, defined as the difference of the measured conductance, G, and the dc conductance, $G_{dc}$, obtained by differentiating the measured I - V curve. It also shows the excess noise conductance, $G_{ex}$, as difference of the measured noise conductance, $G_{eq}$, and its extrapolation into the bump region. The curves $G_{ac}$ and $G_{ex}$ of samples 1 and 3 exhibit a

similar bias dependence since both are caused by interface states [21]. This proves again the close relationship between low frequency noise and surface states.

## 5. CONCLUSIONS

The feasibility of simultaneous and independent measurements of low frequency noise and surface state properties of MOS diodes with 20 - 40 Å thick oxide layers has been shown. A simple theoretical model explains qualitatively the experimental results. Continuation of this work in a Ph.D. thesis is expected to reveal further details of the relation between low frequency noise and surface states. Both should depend on sample material and processing.

## Appendix A. Measuring Precautions

During the experiments, the following precautions were taken:

1. To avoid pick up of disturbances from the 60 Hz line and other external electromagnetic sources, the noise measurements were performed in a shielded room, and all instruments and their connections were carefully shielded.

2. To reduce stray capacitances particularly at the preamplifier input that increase the amplifier noise (cf. Appendix D), all connecting cables were kept as short as possible.

3. To check that the amplifier operated in its linear region and was never saturated, its output was displayed on an oscilloscope. If the output signal was clipped, the amplifier gain was reduced and/ or its lower cut off frequency increased.

4. Since low frequency noise components can drive the wave analyzer into saturation where it is not calibrated, these components were cut off from the amplifier input when small high frequency components were measured.

5. The signal generator was comletely disconnected in switch off condition to avoid its residual voltage.

6. To avoid undesired noise contributions, all instruments not employed during noise measurements were also disconnected from the circuit. This is particularly important for the Keithley Electrometer that produces a high noise level.

## Appendix B. Effective Noise Bandwidth

The wave analyzer is calibrated by the manufacturer for a sinusoidal input; however, the measured noise voltage has a normal

time distribution. This fact is taken into account by defining an effective noise bandwidth of the wave analyzer,

$$B = (1/|A_o|^2)\int_0^\infty |A(f)|^2 \, df, \tag{B1}$$

A(f) is its voltage gain with input shorted, and $A_o$ the maximum value of A(f).

To measure the effective noise bandwidth, the admittance, $Y_s$, in Fig. 22 is replaced by a large resistor $R_s$ producing thermal noise of such magnitude that the amplifier noise is neglegible. Then the noise current $I_{tot}$ is measured as outlined in Section 3.21 resulting in

$$I_{tot}^2 = 4kT(1/R_s)\, B \quad , \tag{B2}$$

and

$$B = I_{tot}^2 R_s/(4kT) \, . \tag{B2a}$$

Using eqs. (3.6a) and (B2a) yields the desired quantity

$$B = V_s^2 R_s/(4kTN^2|Z|^2) \, . \tag{B2b}$$

The wave analyzer QTL 303, set at 10 Hz signal bandwidth, exhibited an effective noise bandwidth,

$$B = 8.8 \pm 0.5 \text{ Hz} \, , \tag{B3a}$$

while the HP 302 AR wave analyzer had a noise bandwidth,

$$B = 2.05 \pm 0.1 \text{ Hz}. \tag{B3b}$$

## Appendix C. Amplifier Noise Figure

The amplifier noise figure depending on frequency and source admittance, $Y_s$ $(= G_s + j\omega C_s)$, was determined in two ways; first, by comparing the thermal noise of the source admittance with a signal current source parallel to $Y_s$ and second, with a signal voltage source in series with $Y_s$.

In the first case, the rms noise current, $I_{tot}$, is determined using the set-up of Fig. 22, cf. Section 3.21. Using eqs. (3.1) and (3.6) yields

$$\frac{I_{tot}^2}{4\,G_s} = \frac{4kTG_sB}{4\,G_s} + kT(F-1)B, \qquad (C1)$$

hence,

$$F = \frac{I_{tot}^2}{4kTG_sB} = \frac{(V_s/N|Z|)^2}{4kTG_sB} \; . \qquad (C2)$$

where F is the amplifier noise factor.

In the second case, the signal generator voltage in the set-up of Fig. 23 is set to zero and the amplifier output voltage, $V_n$, noted. Then the signal generator voltage is adjusted to $V_{s1}$ such that the amplifier out put voltage becomes $NV_n$. According to Section 3.21 the power relation,

$$\frac{V_{s1}^2 \times 10^{-8}}{4Re(1/Y_s)} = (N^2-1)\frac{4kTRe(1/Y_s)B}{4Re(1/Y_s)} + kT(F-1)B \; , \qquad (C3)$$

the noise factor,

$$F = \frac{V_{s1}^2 \times 10^{-8}}{(N^2-1)} \times \frac{1}{4kTRe(1/Y_s)B} \; . \qquad (C4)$$

The noise figure,

$$NF = 10\,\log_{10}(F) \; , \qquad (C5)$$

is obtained from eqs. (C2) and (C4).

To determine F from eq. (C5), the exact values of both the source capacitance, $C_s$, and the conductance, $G_s$, have to be known while eq. (C2) does not require knowledge of $C_s$. Application of a current source, cf. equation (C2), is advantageous since connecting cables usually add unknown contribution to $C_s$.

## Appendix D. Preamplifier Properties

The preamplifier PAR 113 has a voltage gain continuously variable from 10 to 25000 at an input impedance of 100 Mohm shunted by a 15 pF capacitance. Its lower cut off frequency is variable between 0.03 Hz and 1 kHz and its upper cut off frequency between 3 Hz and 300 kHz. To measure the amplifier voltage gain,

$$A_v = A_o \, Z_i/(Z_i + Z_s) = A_o \, Y_s/(Y_i + Y_s) \, , \qquad (D1)$$

as function of frequency and source admittance, the set-up of Fig. 23 is used. $A_o$ is the voltage gain with shorted amplifier input, $Z_i$ the input impedance, $Z_s$ the source impedance, $Y_i$ the input admittance, and $Y_s$ the source admittance of the amplifier. The gain $A_v$ for resistive $Z_s$ depends strongly on frequency as shown in Fig. 24. It reduces at high frequencies, cf. eq. (D1), to

$$A_v = A_o \, C_s/(C_i + C_s) \, , \qquad (D2)$$

a function of the amplifier input and source capacitances, $C_i$ and $C_s$, but independent of frequency and source resistance, $R_s$. This behavior is shown in Fig. 25.

The measured amplifier noise figure as function of frequency and source impedance is presented in Fig. 26a employing a signal current source and in Fig. 26b employing a signal voltage source. Since the noise figure increases at high frequencies with increasing $C_s$, this capacitance is kept small by using short connecting cables.

## Appendix E. Simulation of Diode Admittance

The diode admittance is simulated by an admittance, $Y_s$, which consists of a resistor $R_s$, variable between 1 kohm and 87 Mohm, and a capacitor $C_s$, variable between 5 pF and 400 pF. To obtain the simulation admittance above 5 kHz, the Boonton 75-CS capacitance

bridge which allows differential C-,G-measurements was used, adjusting both $R_s$ and $C_s$ so that the differential capacitance and conductance between diode and admittance box became zero.

To obtain $Y_s$ for frequencies below 5 kHz, the set-up of Fig. 5 was employed. An ac signal current of the measuring frequency was applied to the biased diode and the developed voltage noted. Then, the same ac current was applied to the admittance box, and the resistance $R_s$ adjusted so that the measured voltage drop appeared again across the admittance. $C_s$ was kept at its value determined at 5 kHz, since an inspection of the diode C-V curves proved that the diode capacitance did not change much at low frequencies.

REFERENCES

1. A. van der Ziel," Noise in Solid State Devices and Lasers", Proc. IEEE, 58,1178-1206,1970.

2. C.T.Sah,"Theory of Low Frequency Generation Noise in Junction Field Effect Transistors", Proc. IEEE, 51,795-814,1964.

3. P.O.Lauritzen,"Low Frequency Generation Noise in JFETs", Solid St. Electron.,8,41-58,1965.

4. S.Y.Wu,"Theory of Generation - Recombination Noise in MOS Transistors", Solid St. Electron.,11,25-32,1968.

5. L.D.Yau,C.T.Sah,"Theory and Experiment of Low Frequency Noise in MOS Transistors", IEEE Trans. Elec. Dev., ED-16,170-177,1969.

6. A.L.McWhorter,"1/f Noise and Germanium Surface Properties", "Semiconductor Surface Physics",ed.-R.H.Kingston, U of Penn. Press, 1957.

7. C.T.Sah,F.H.Hielscher,"Evidence of Surface Origingof the 1/f Noise", Phys. Rev. Letter, 17,956-958,1966.

8. G.Abowitz,E.Arnold,E.Leventhal,"Surface States and 1/f Noise in MOS Transistors", IEEE Trans. Elec. Dev., ED-14,775-776,1967.

9. S.T.Hsu,D.J.Fitzgerald,A.S.Grove,"Surface States Related 1/f Noise in P-N Junctions and MOSTs",Appl.Phy,Lett.,12,287-289,1968.

10. E.A.Leventhal,"Derivation of 1/f Noise in Silicon Inversion Layer from Carrier Motion in a Surface Band", Solid St. Electron., 11,621-627,1968.

11. O.Jantsch,"A Theory of 1/f Noise at Semiconductor Surfaces", Solid St. Electron., 11,267-272,1968.

12. S.Christensson,I.Lundstrom,C.Svensson,"Low Frequency Noise in MOS Transistors - I", Solid St. Electron.,11,792-812,1968.

13. S.T.Hsu,"Surface State Related 1/f Noise in MOS Transistors", Solid St. Electron.,13,1451-1459,1970.

14. F.Berz,"Theory of Low Frequency Noise in Silicon MOSTs", Solid St. Electron.,13,631-647,1970.

15. I.Flinn,G.Bew,F.Berz,"Low Frequency Noise in MOS Field Effect Transistors",Solid St. Electron.,10,833-845,1967.

16. I.R.Mansour,R.J.Hawkins,G.G.Bloodworth,"Measurement of Current Noise in MOS Transistors from $5 \times 10^{-5}$ Hz to 1 Hz", Radio Elec. Engr.,35,212-216,1968.

17. S.Christensson,L.Lundstrom,"Low Frequency Noise in MOS Transistors-II", Solid St. Electron.,11,813-820,1968.

18. F.Leuenberger,"1/f Noise in Gate Controlled Planar Silicon Diodes", Electron. Lett.,4,280,1968.

19. S.T.Hsu,"Surface State Related 1/f Noise in P-N Junctions", Solid St. Electron.,13,843-855,1970.

20. E.Nicollian,H.Melchior," A Quantitative Theory of 1/f Type Noise Due to Interface States in Thermally Oxidized Silicon", BSTJ,46,2019-2033,1967.

21. S.Kar,"Interface States and Potential Barriers in Metal-(20-50 Å)$SiO_2$-Si Structures", Ph.D. Thesis, Lehigh Univ., 1971.

22. S.Kar,W.E.Dahlke," Metal Dependent Interface States in Thin MOS Structures", Appl. Phy. Lett., 18,401-403,1971.

23. A. van der Ziel,"Noise: Sources, Characterization, Measurements", Prentice Hall, 1970.

24. S.M.Sze,"Physics of Semiconductor Devices", John Wiley & Sons, 1969.

25. E.Nicollian,A.Goetzberger, "The Si-$SiO_2$ Interface Electrical Properties as Determined by the Metal-Insulator-Silicon Conductance Technique", BSTJ,46,1055-1133,1967.

26. W.E.Demming,"Statistical Adjustment of Data", John Wiley & Sons, 1948.

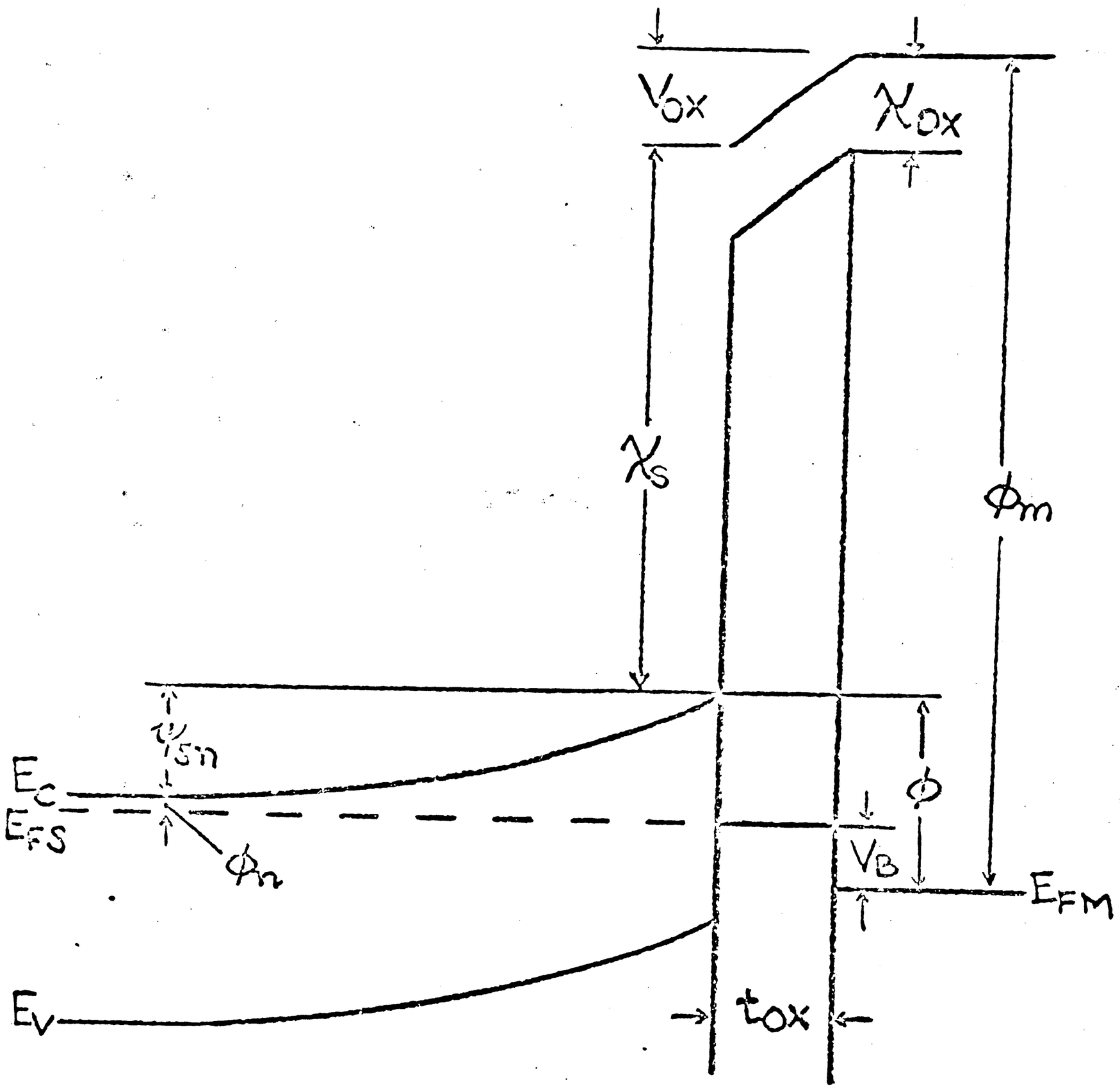


Fig. 1. Energy band model.

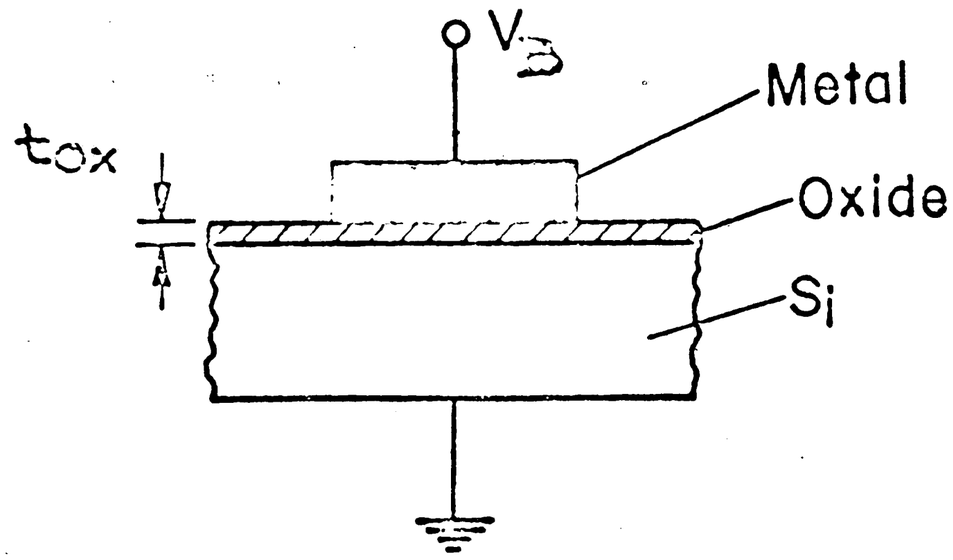


(a)

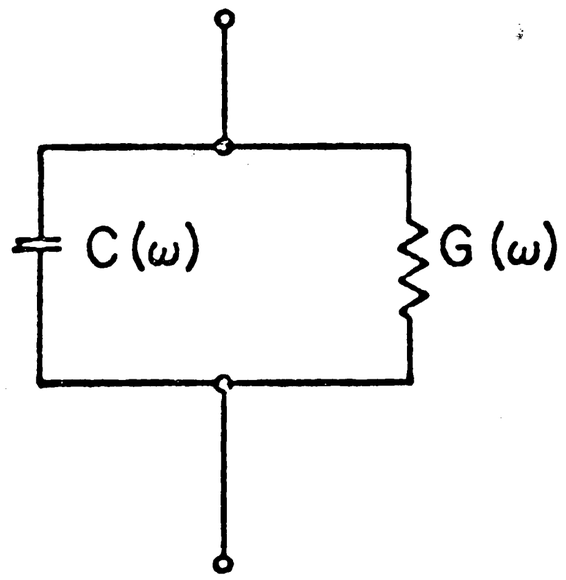


(b)

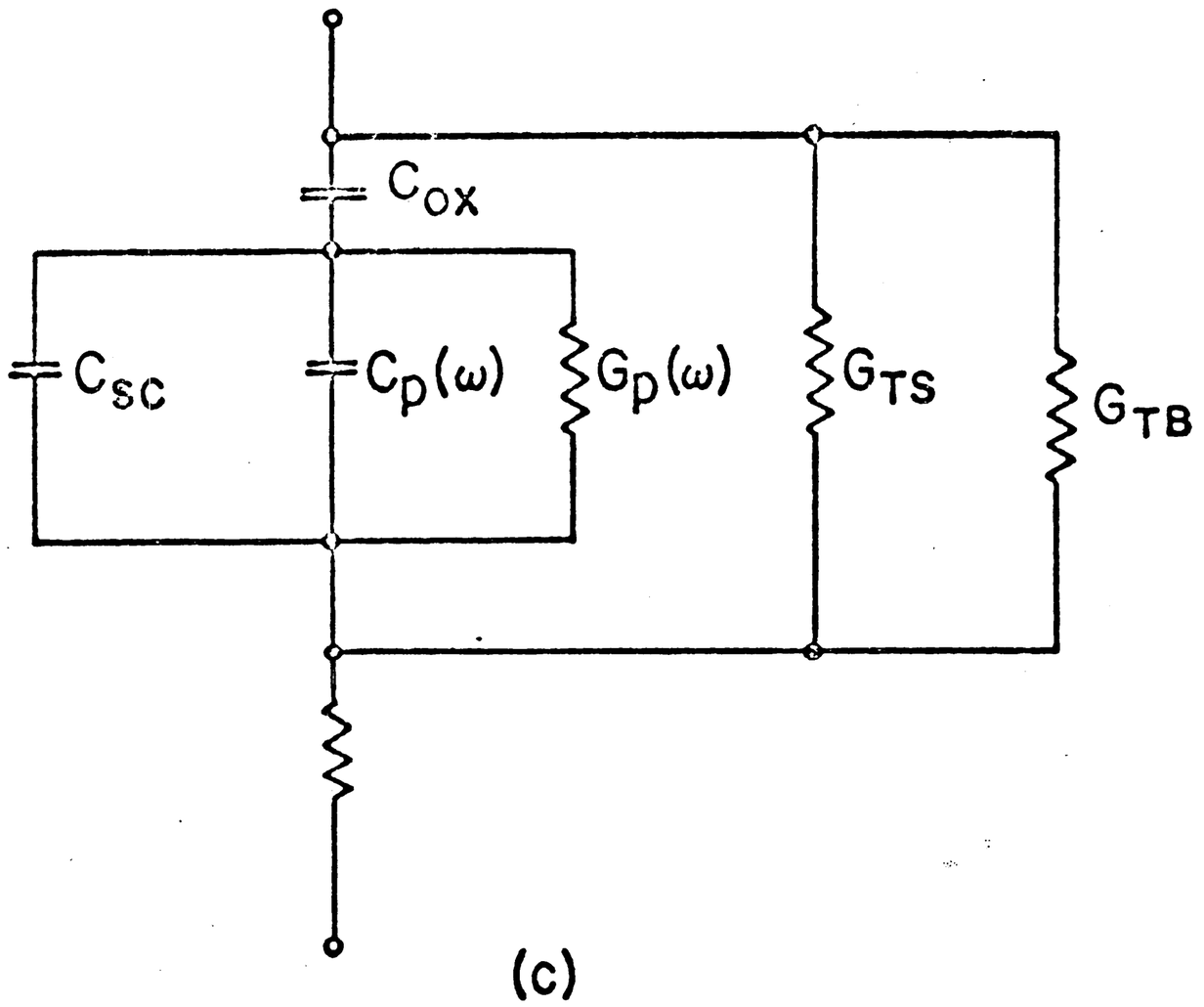


(c)

Fig. 2. MOS structure (a) Physical structure, (b) MOS admittance, (c) Equivalent circuit.

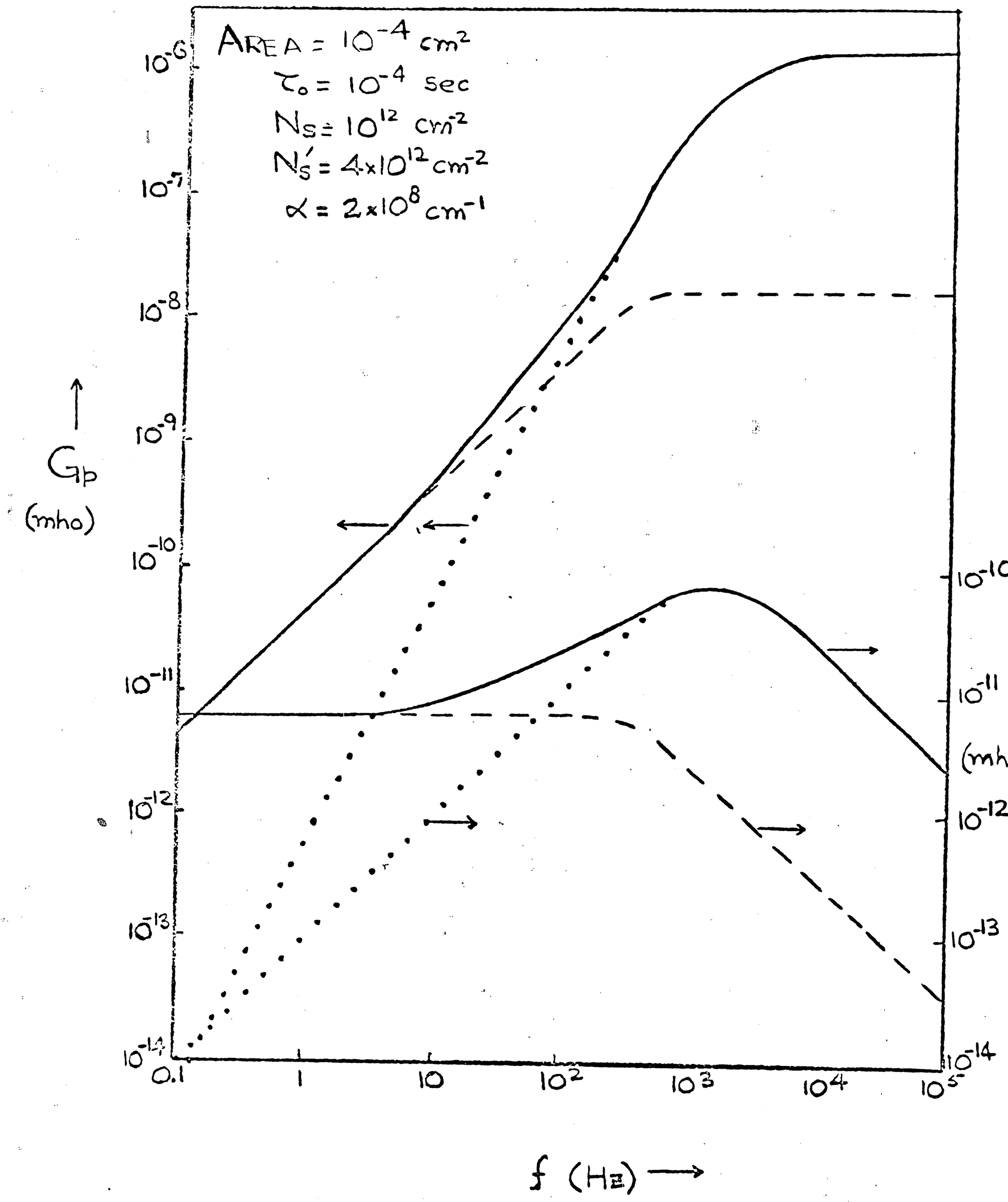


Fig. 3a. Calculated values of $G_p(\omega)$ and $G_p(\omega)/\omega$ .

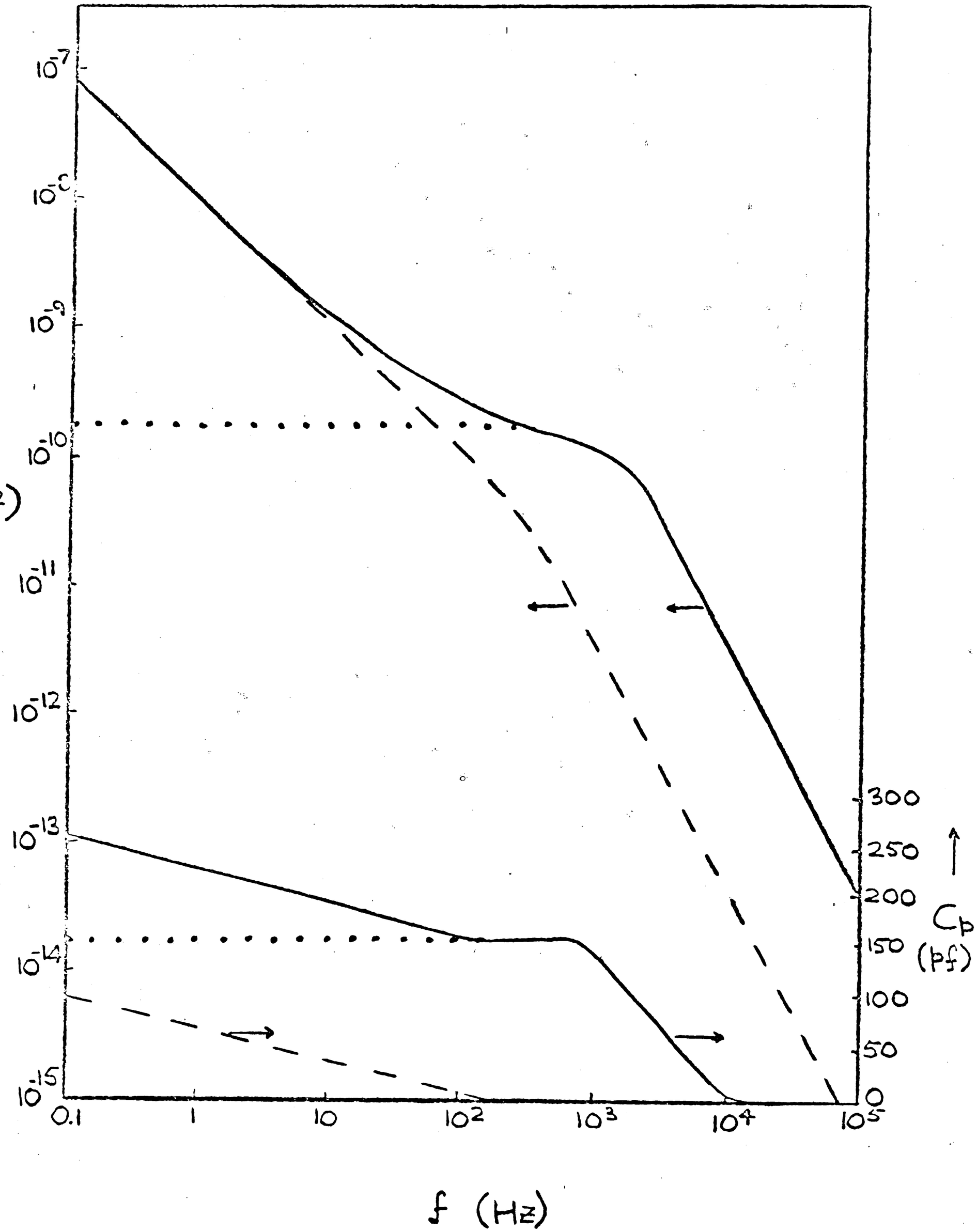


Fig. 3b. Calculated values of $G_p(\omega)/\omega^2$ and $C_p(\omega)$.

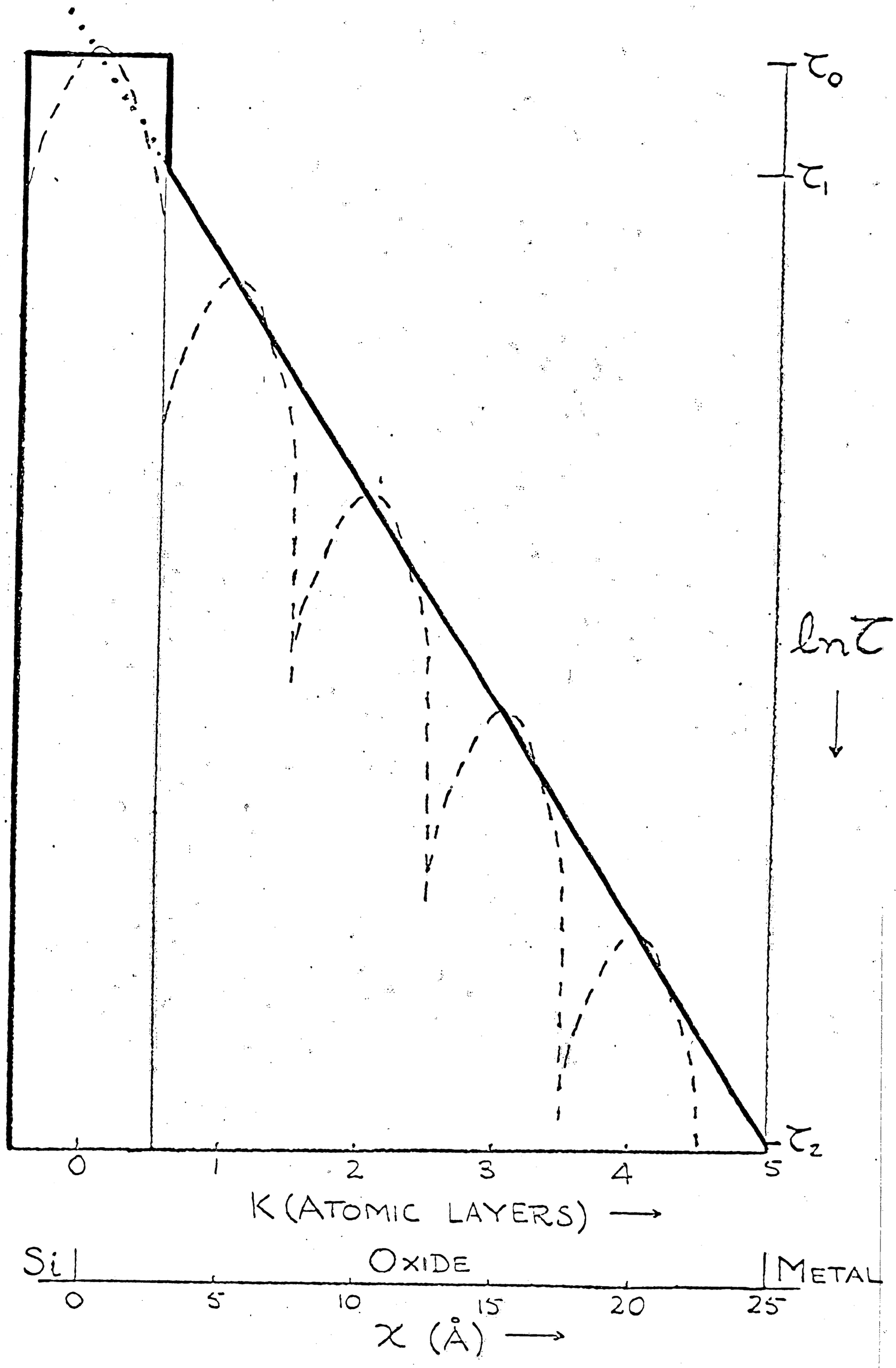


Fig. 4. Assumed distribution of capture cross section and time constant in $SiO_2$.

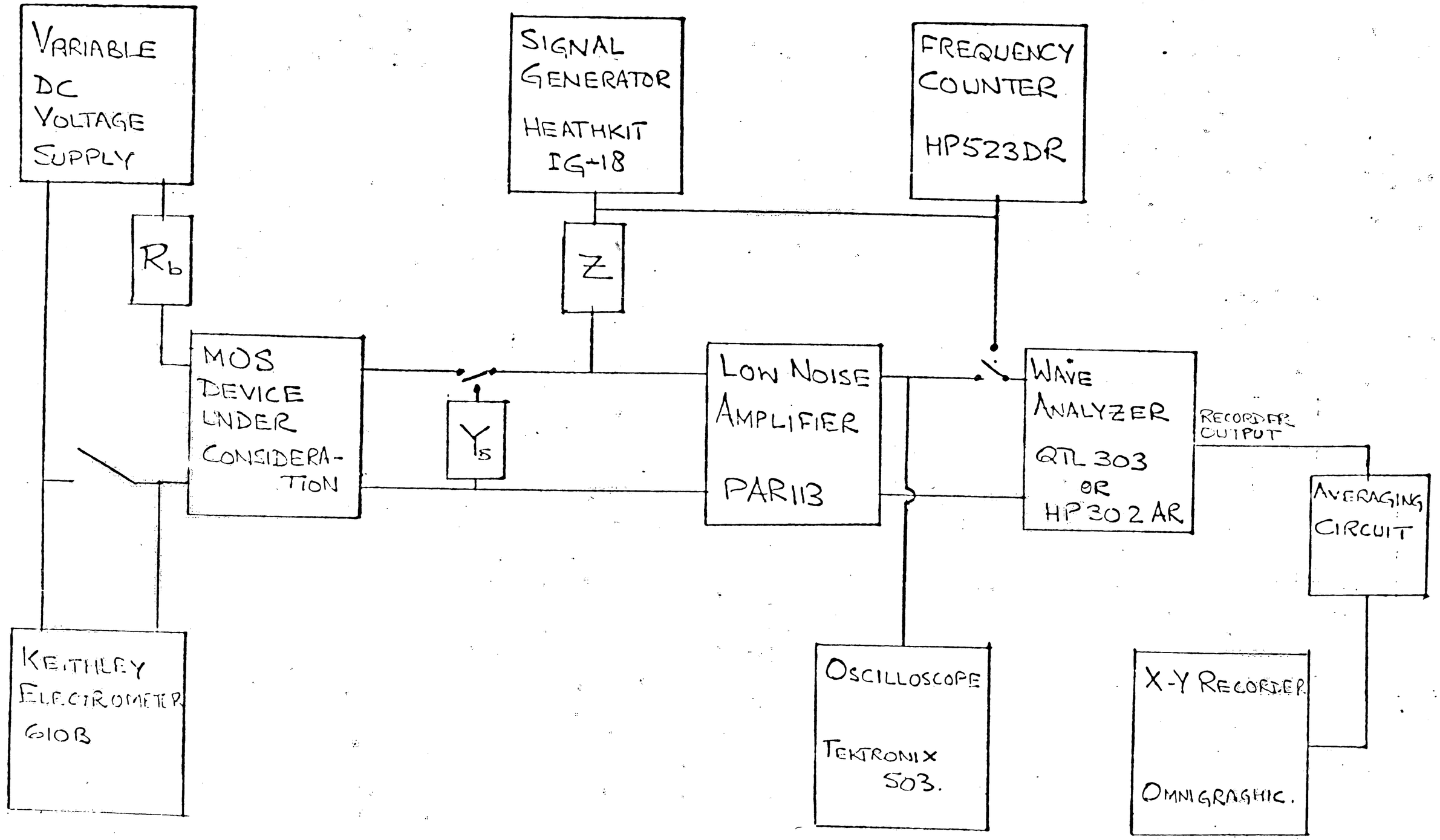


Fig. 5. Noise measurement set-up.

(a)

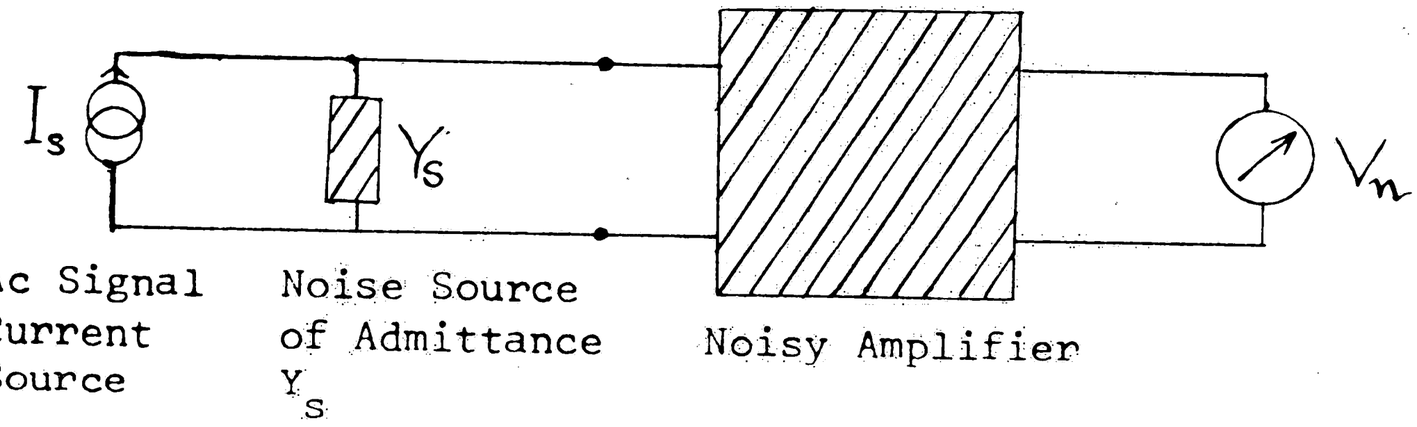


(b)

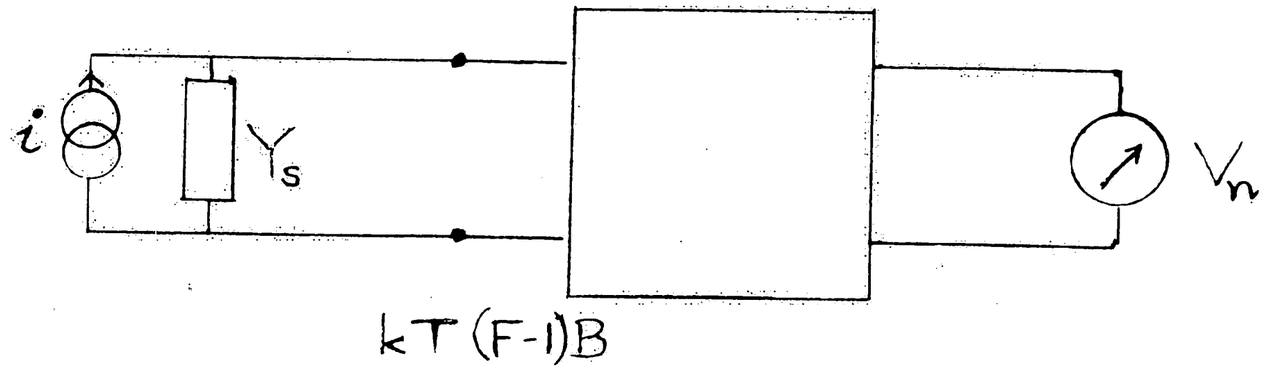


(c)

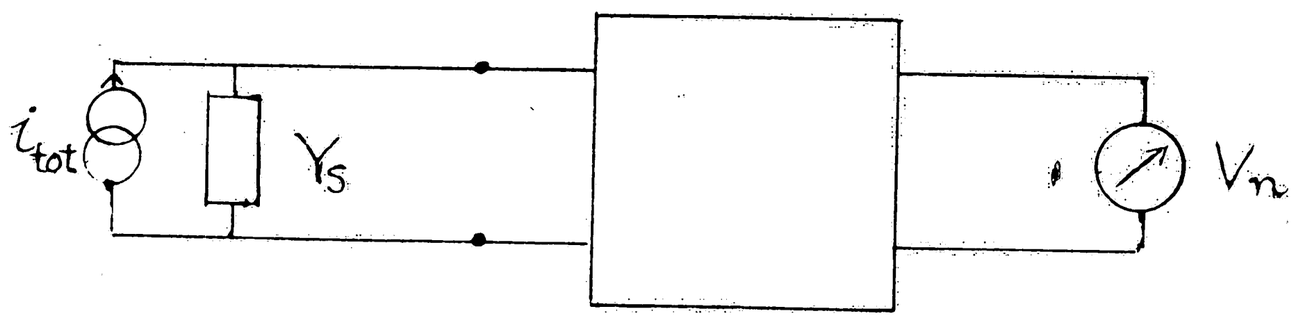


(d)

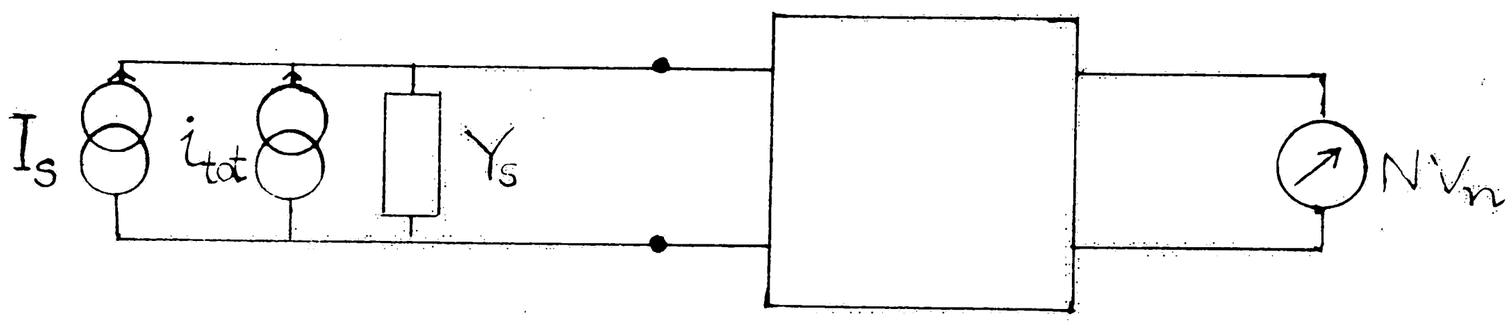


Fig. 6. (a) Basic set-up for measuring $i_{tot}$. (b) Ac signal current source is set zero. The amplifier output voltage is $V_n$. (c) Equivalent input noise circuit. (d) With current source set to $I_s$, the output voltage is $NV_n$.

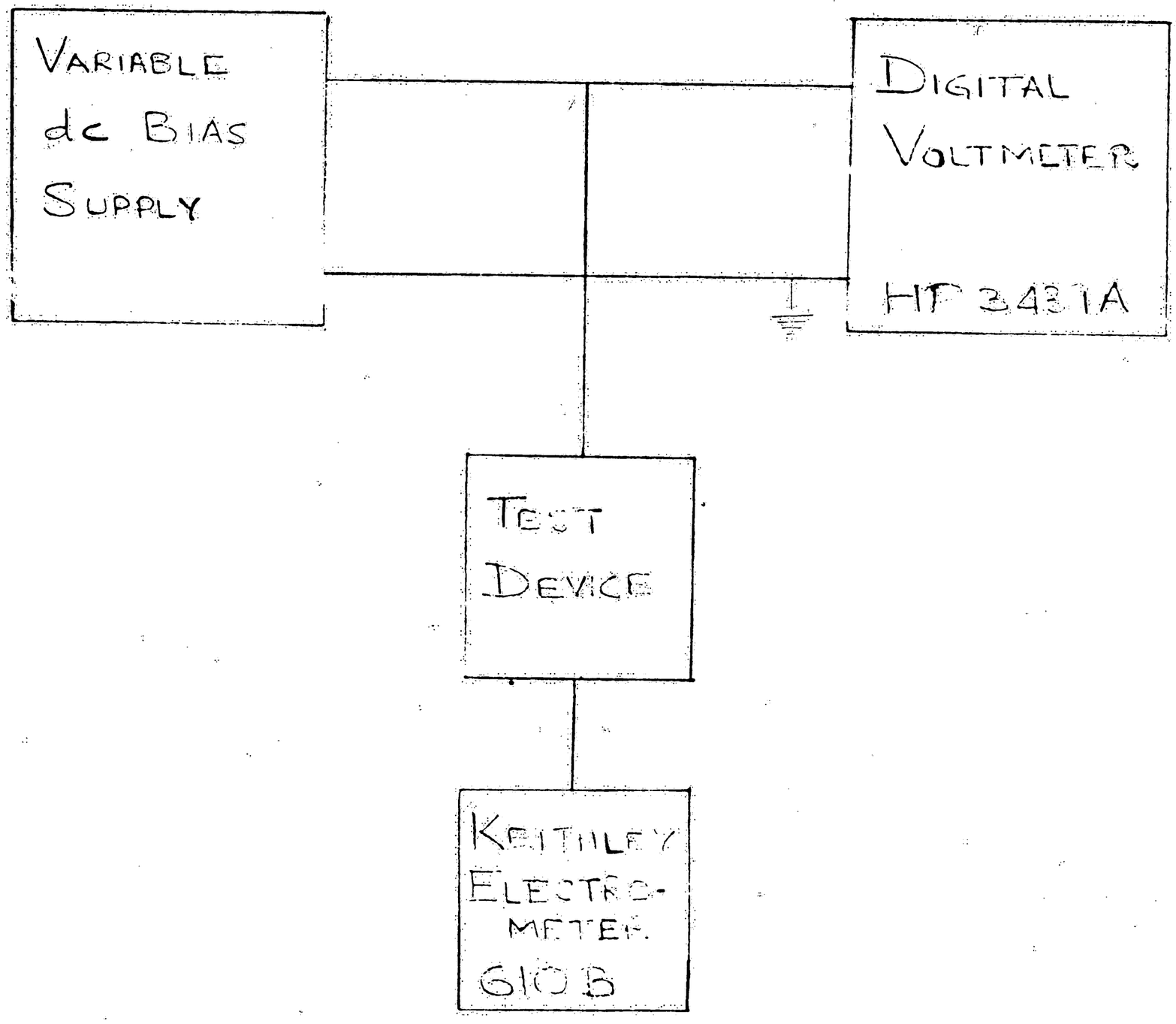


Fig. 7. Set-up used to measure MOS direct current vs. bias characteristic.

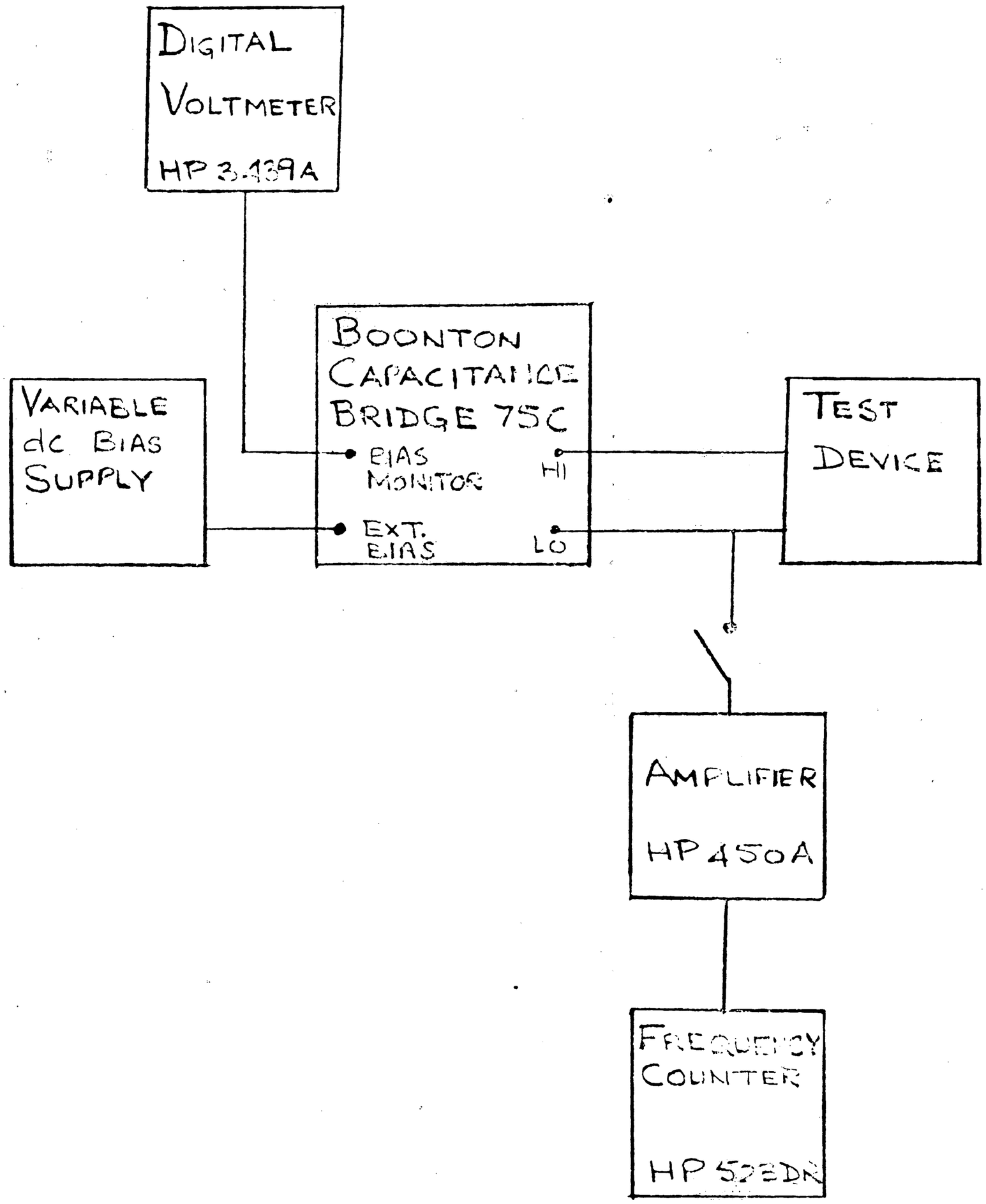


Fig. 8. Set-up used to measure MOS admittance as function of frequency and bias.

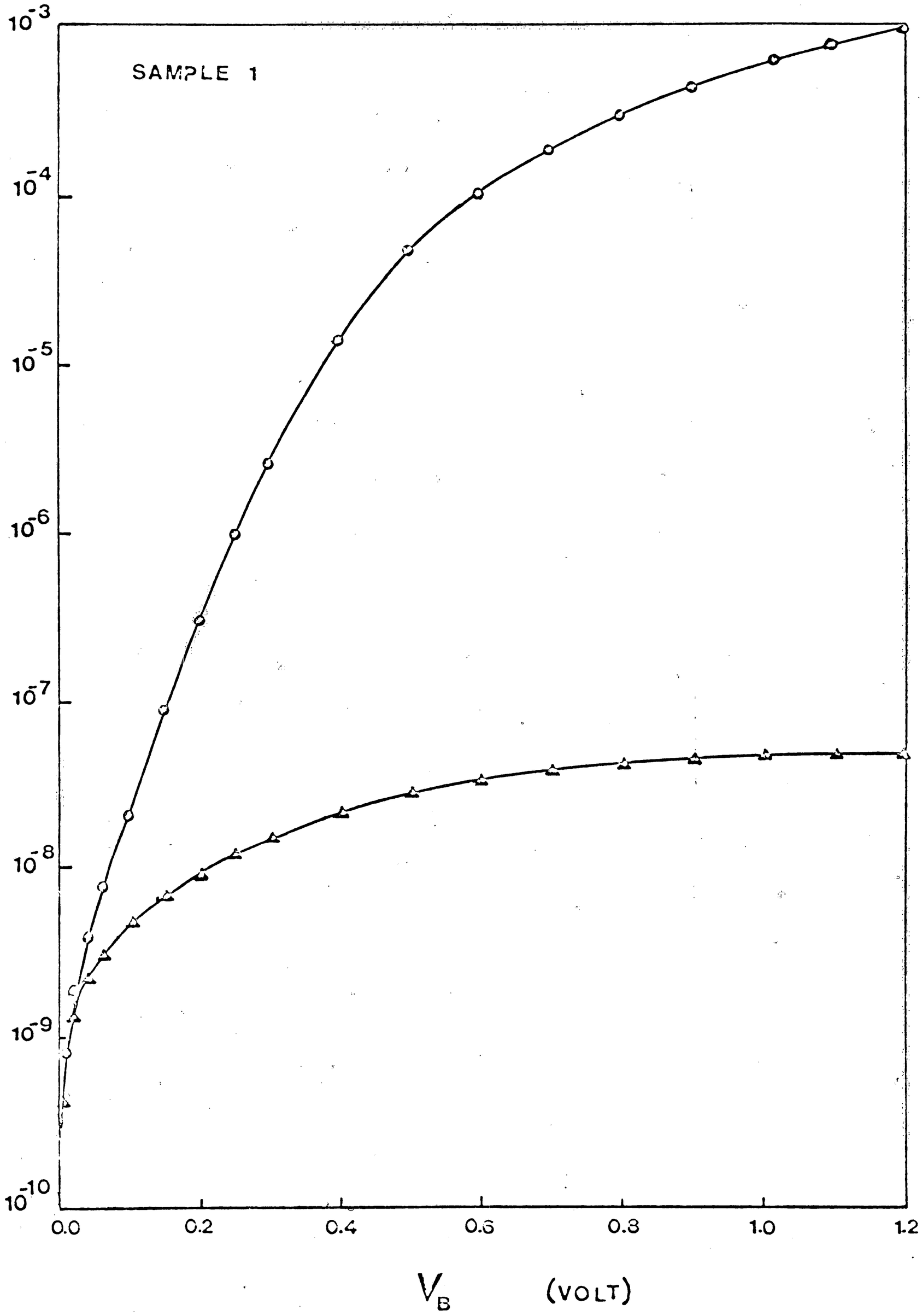


Fig. 9. Measured dc current vs. bias $V_B$ of Sample 1 .

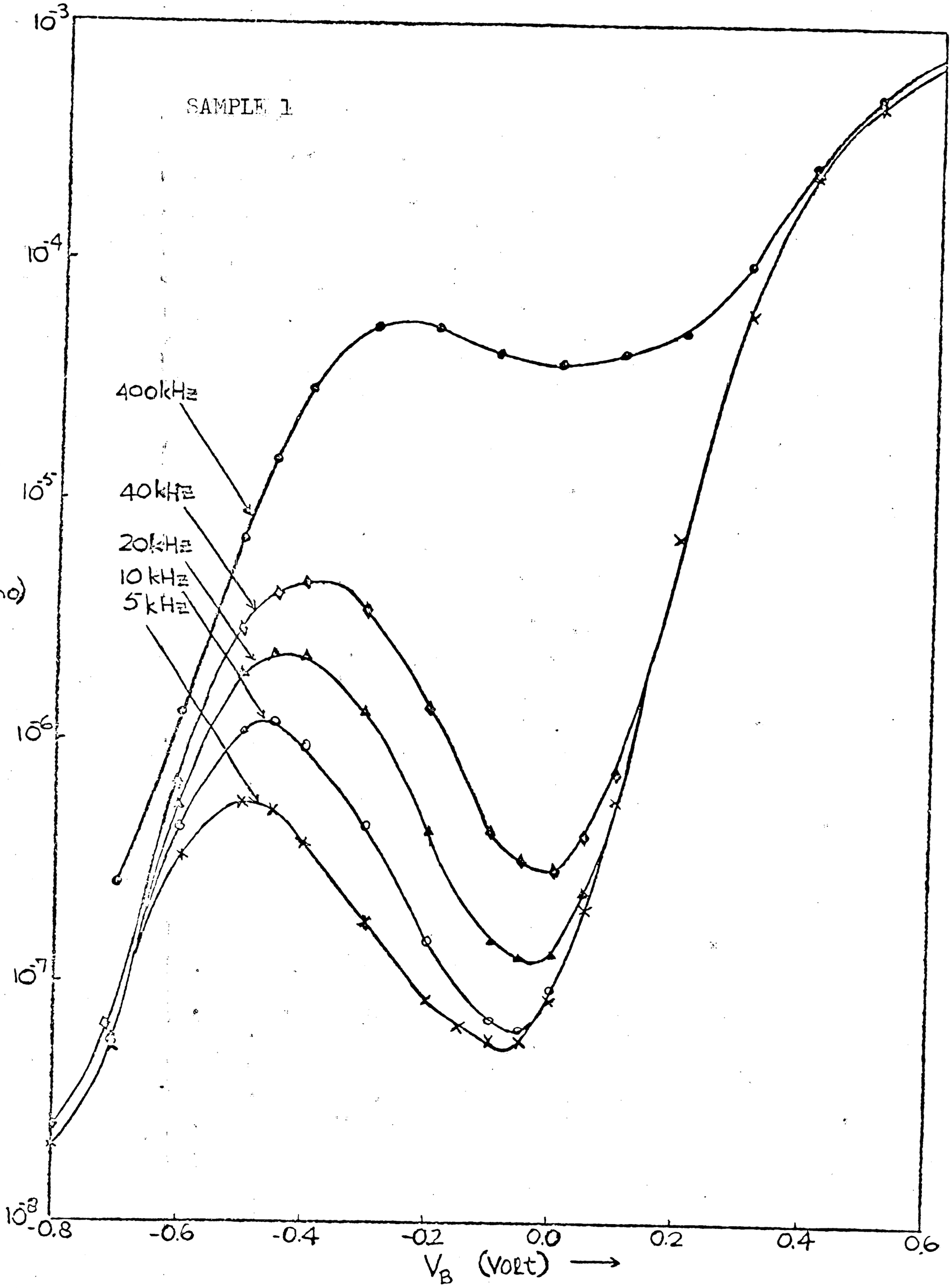


Fig. 10. Measured conductance vs. bias $V_B$ of Sample 1

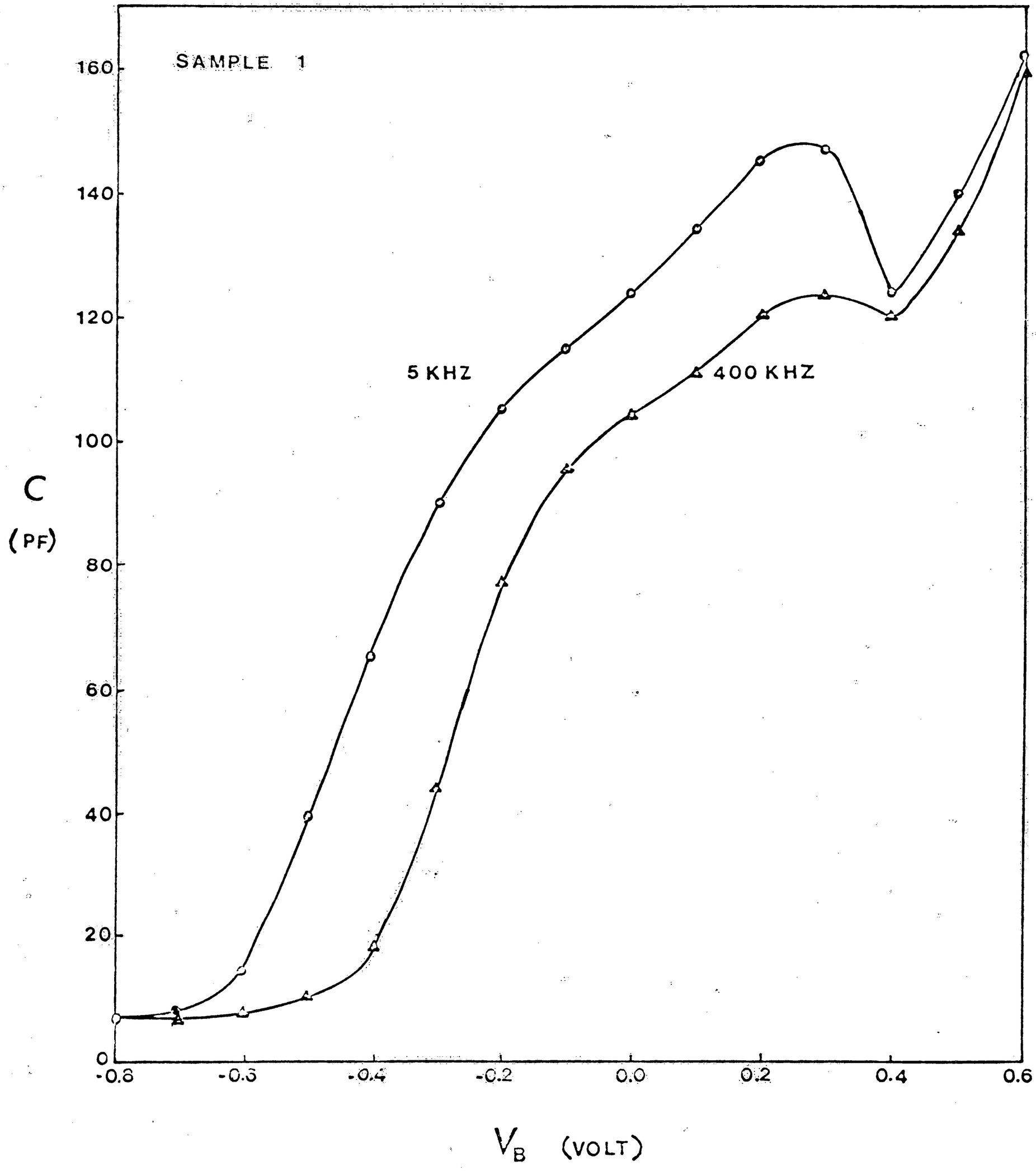


Fig. 11. Measured capacitance vs. bias $V_B$ of Sample 1.

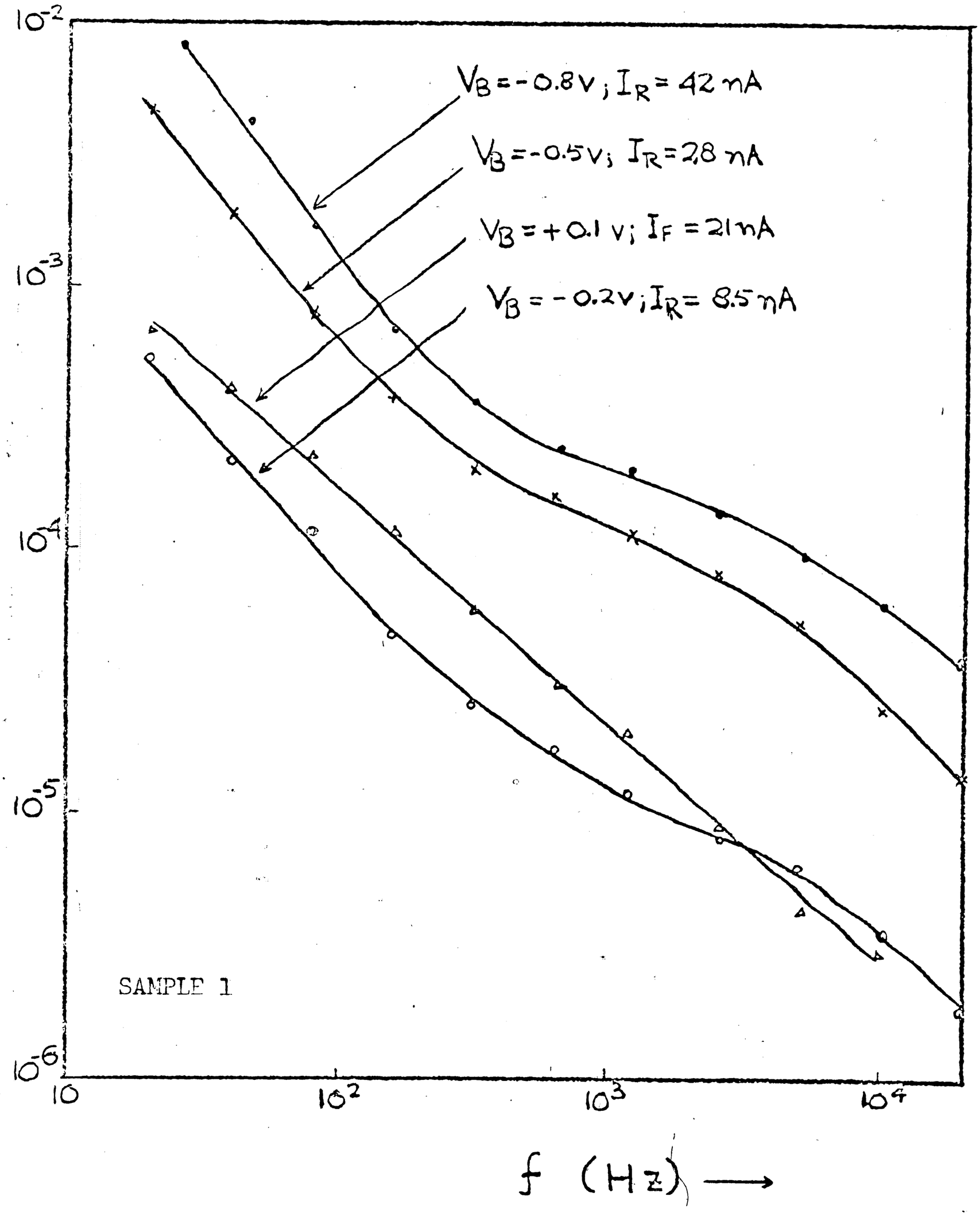


Fig. 12. Measured equivalent noise conductance, $G_{eq}$, vs. f of Sample 1.

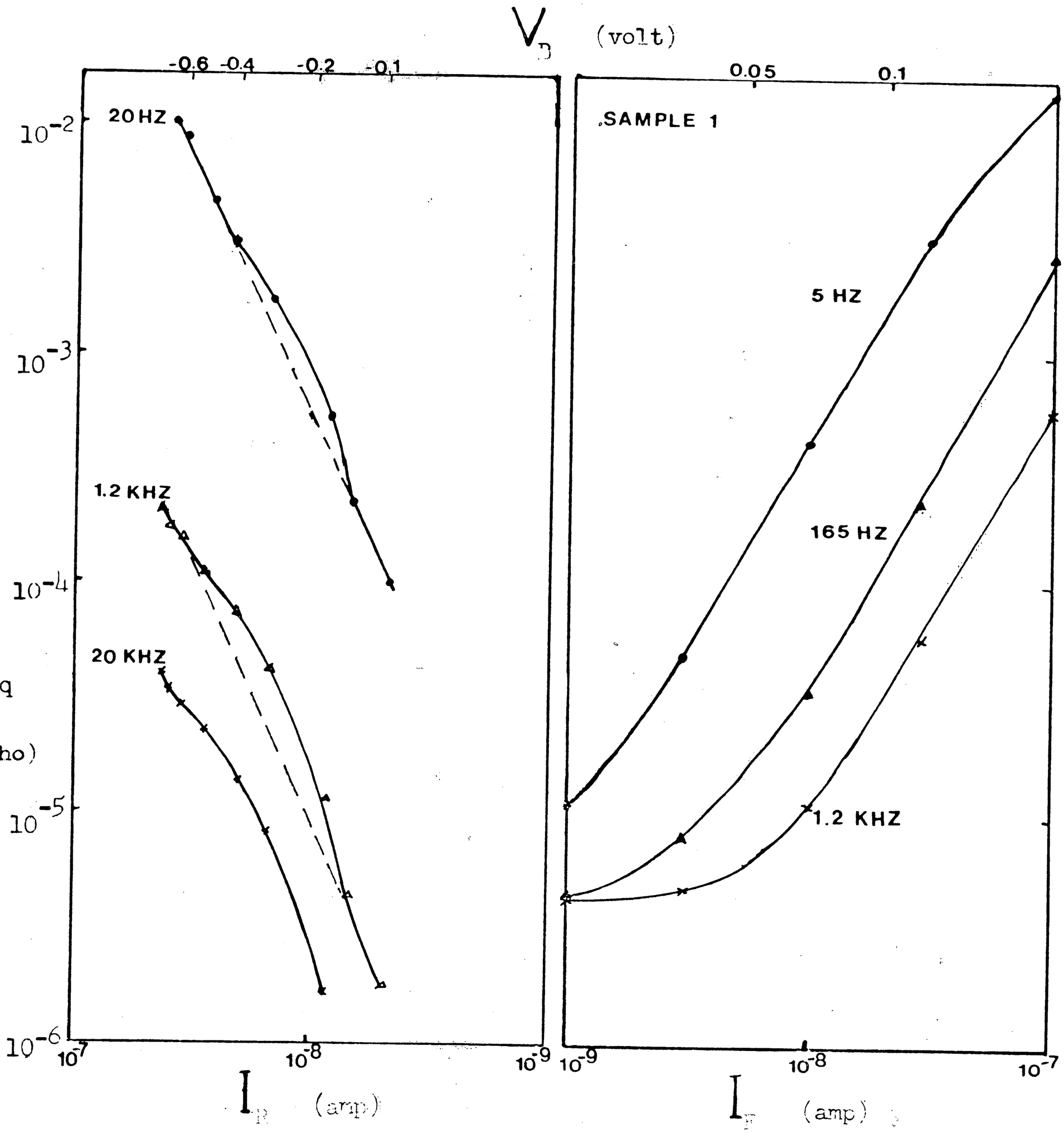


Fig. 13. Measured equivalent noise conductance vs. bias of Sample 1.

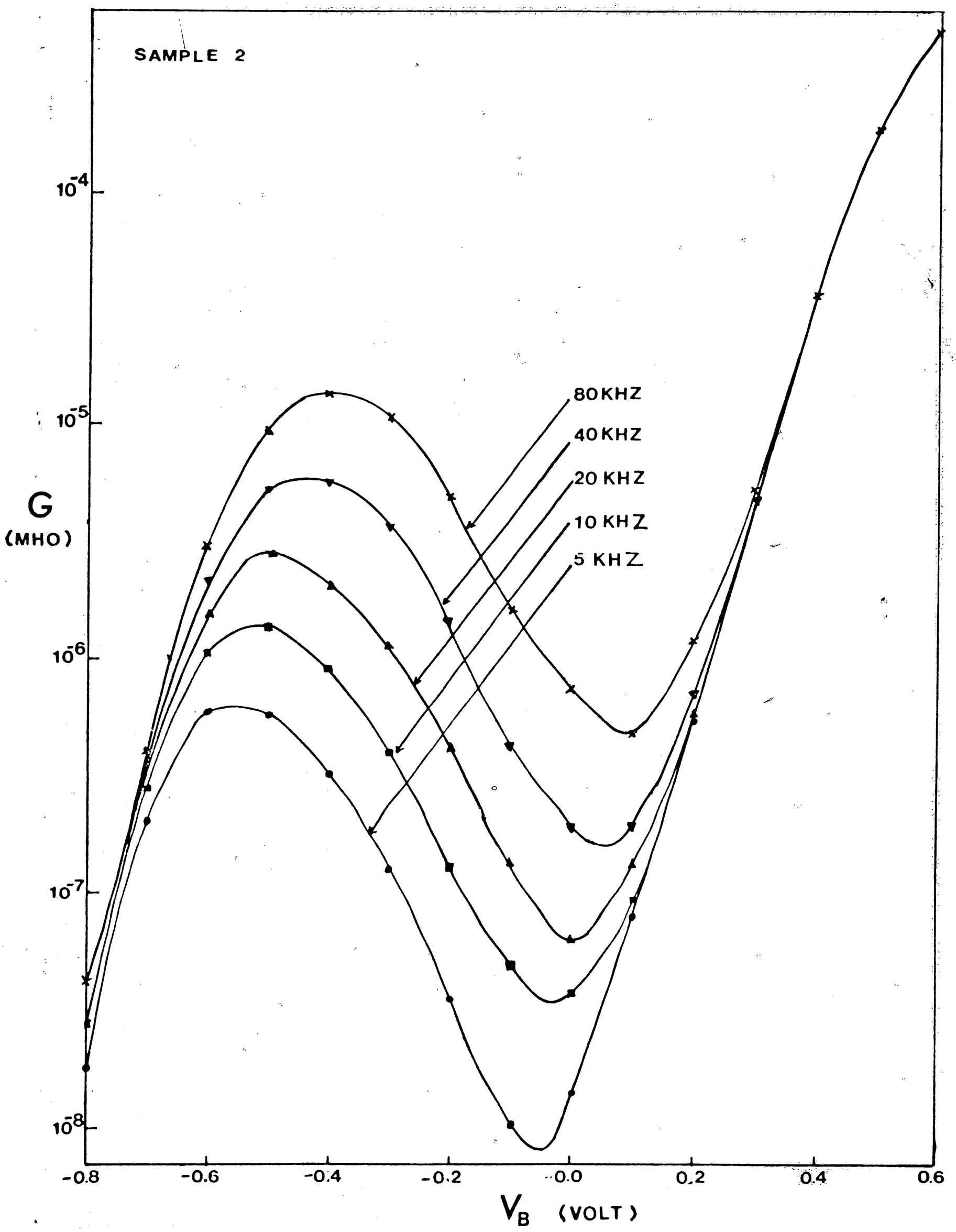


Fig. 11. Measured conductance vs. bias $V_B$ of Sample 2.

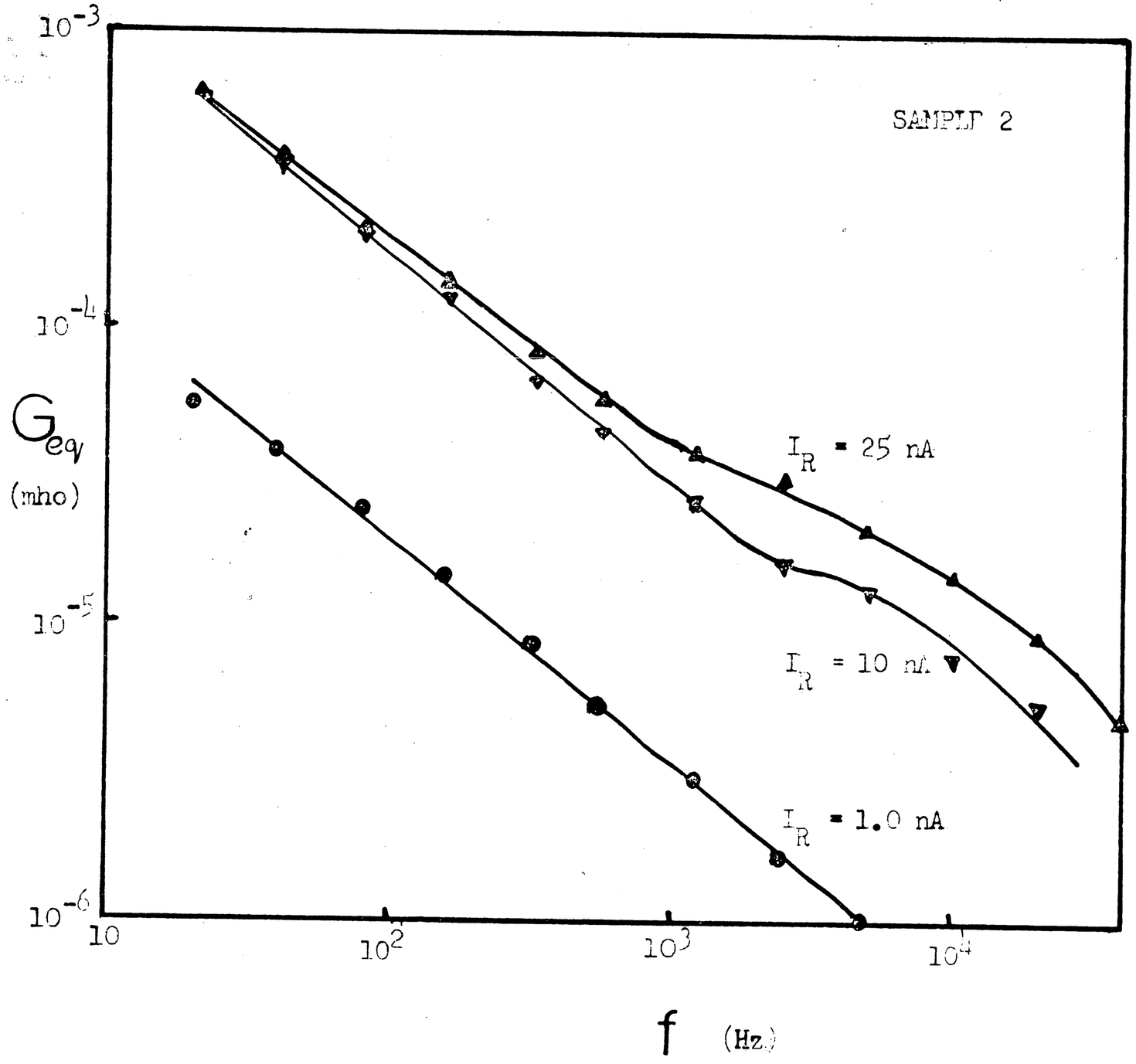


Fig. 15. Measured equivalent noise conductance, $G_{eq}$, vs. f of Sample 1.

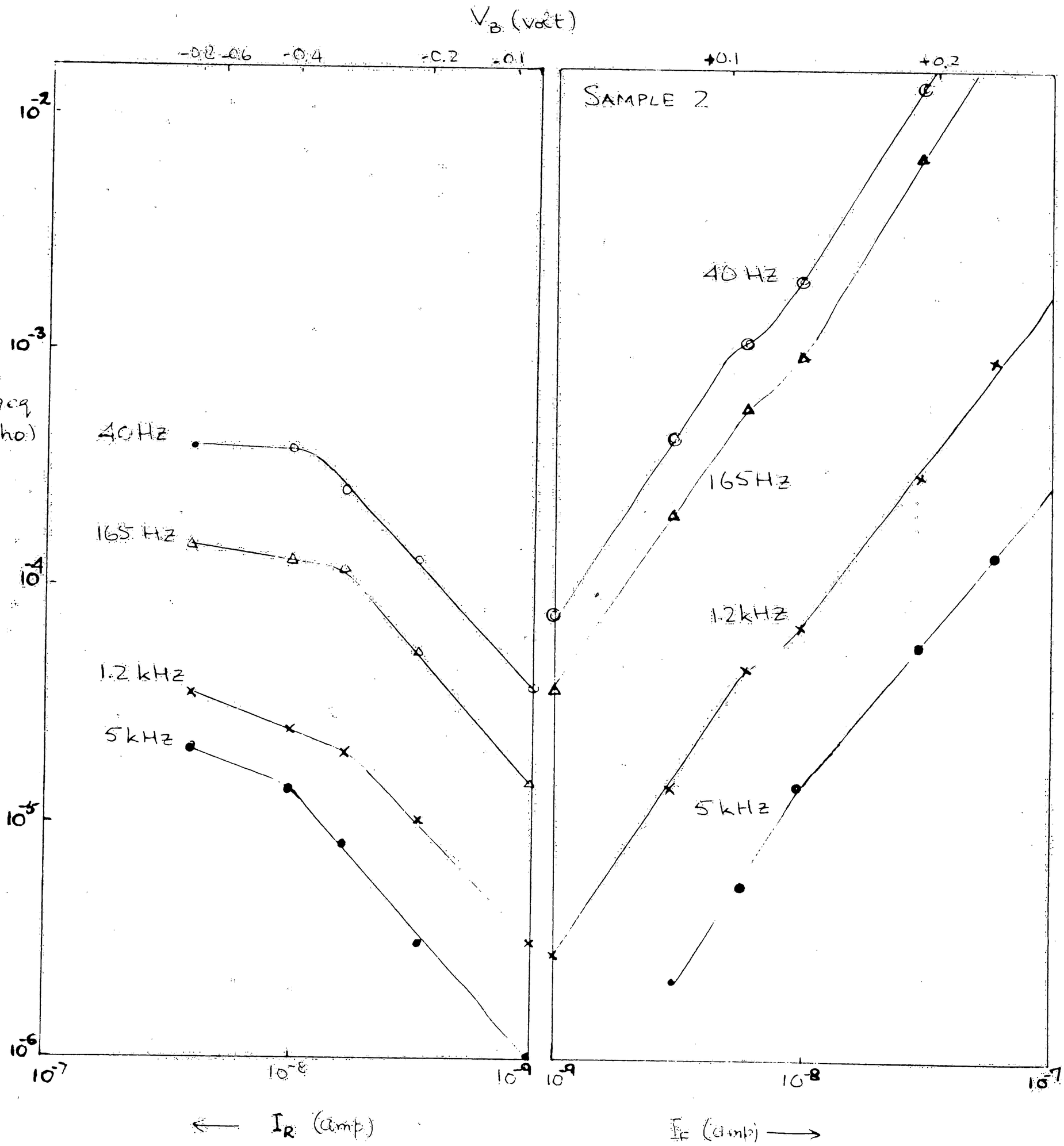


Fig. 16. Measured equivalent noise conductance, $G_{eq}$, vs bias of Sample 2.

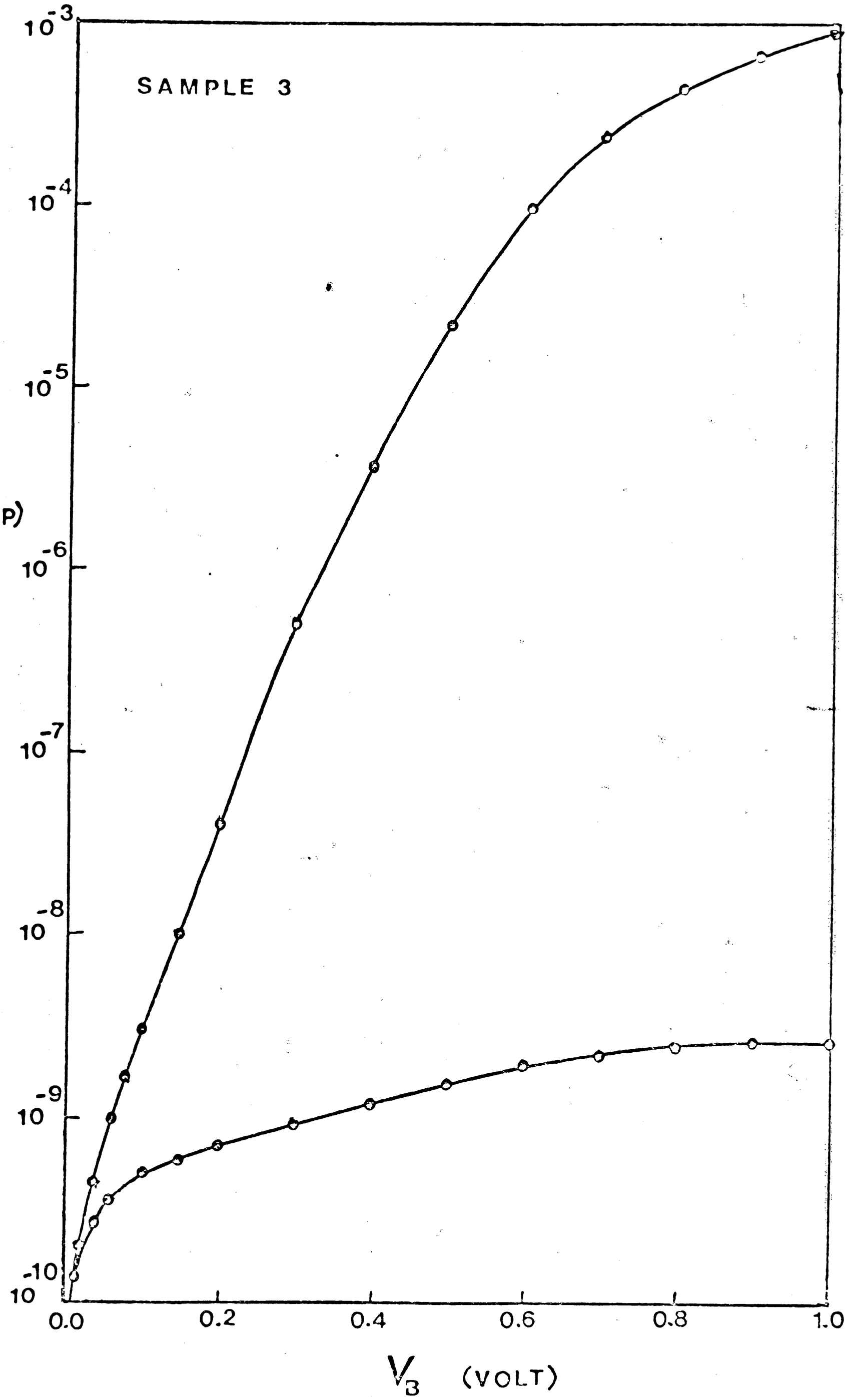


Fig. 17. Measured dc current vs. bias $V_B$ of Sample 3.

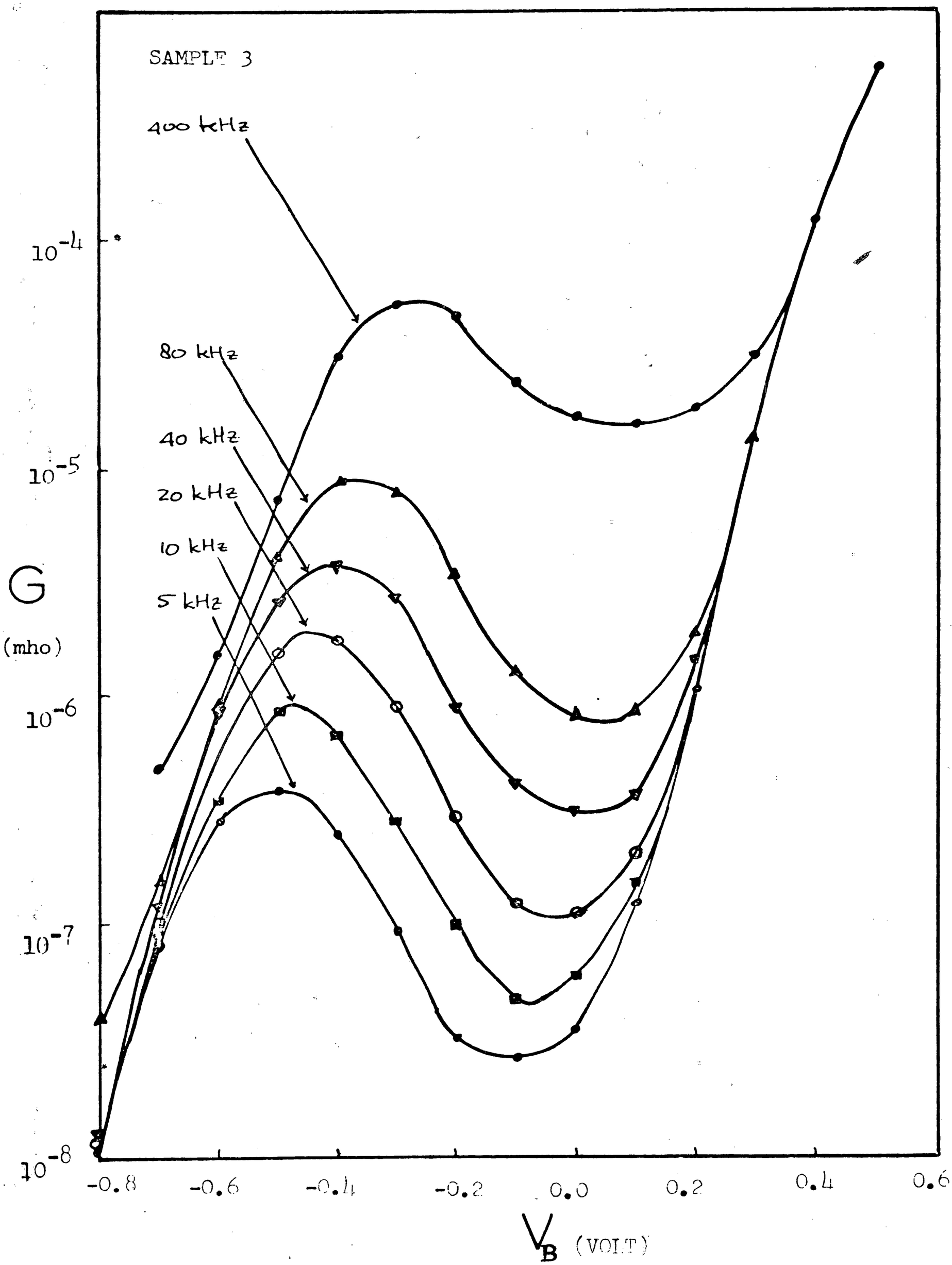


Fig. 18. Measured conductance vs. bias $V_B$ of Sample 3.

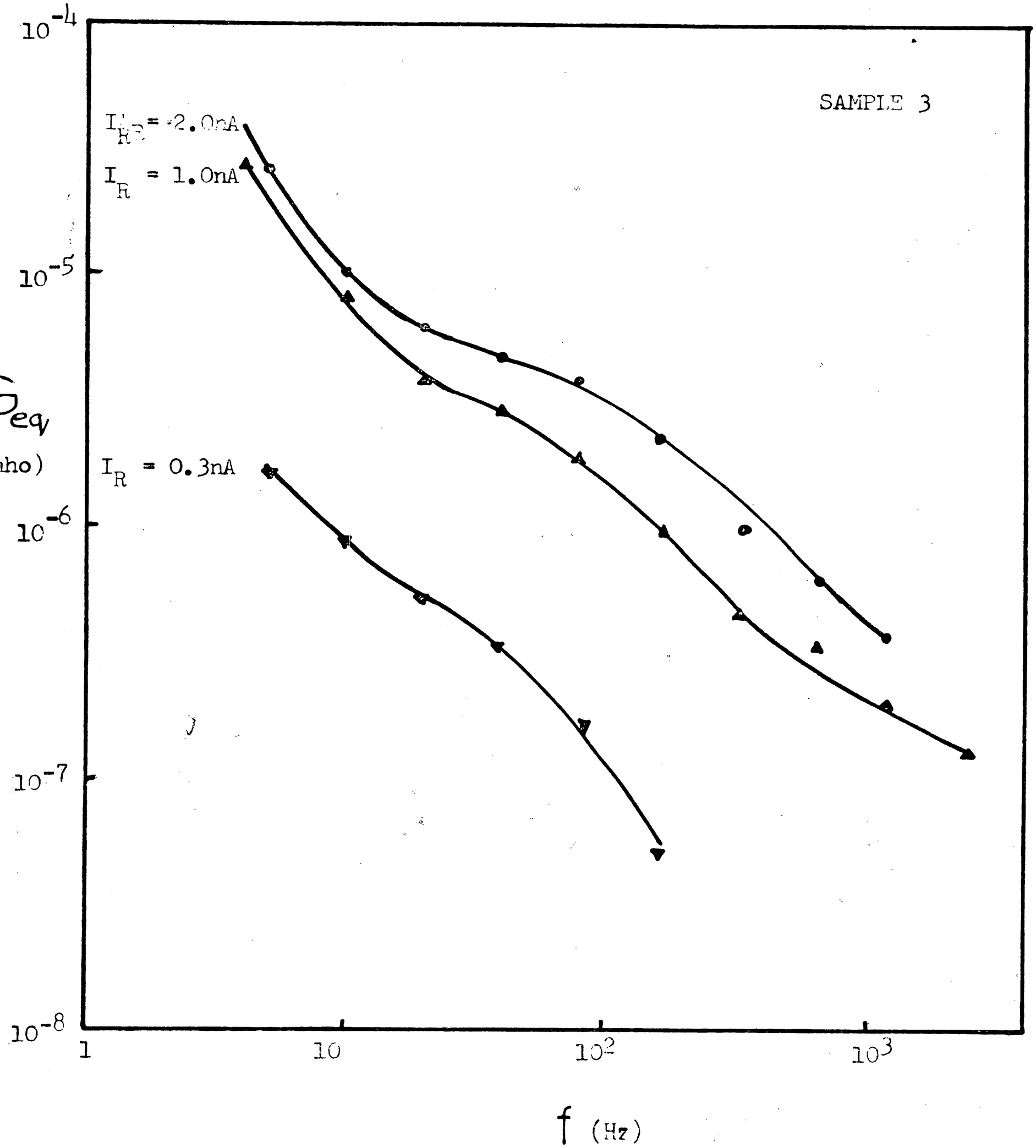


Fig. 19. Measured equivalent noise conductance, $G_{eq}$, vs. f of Sample 3.

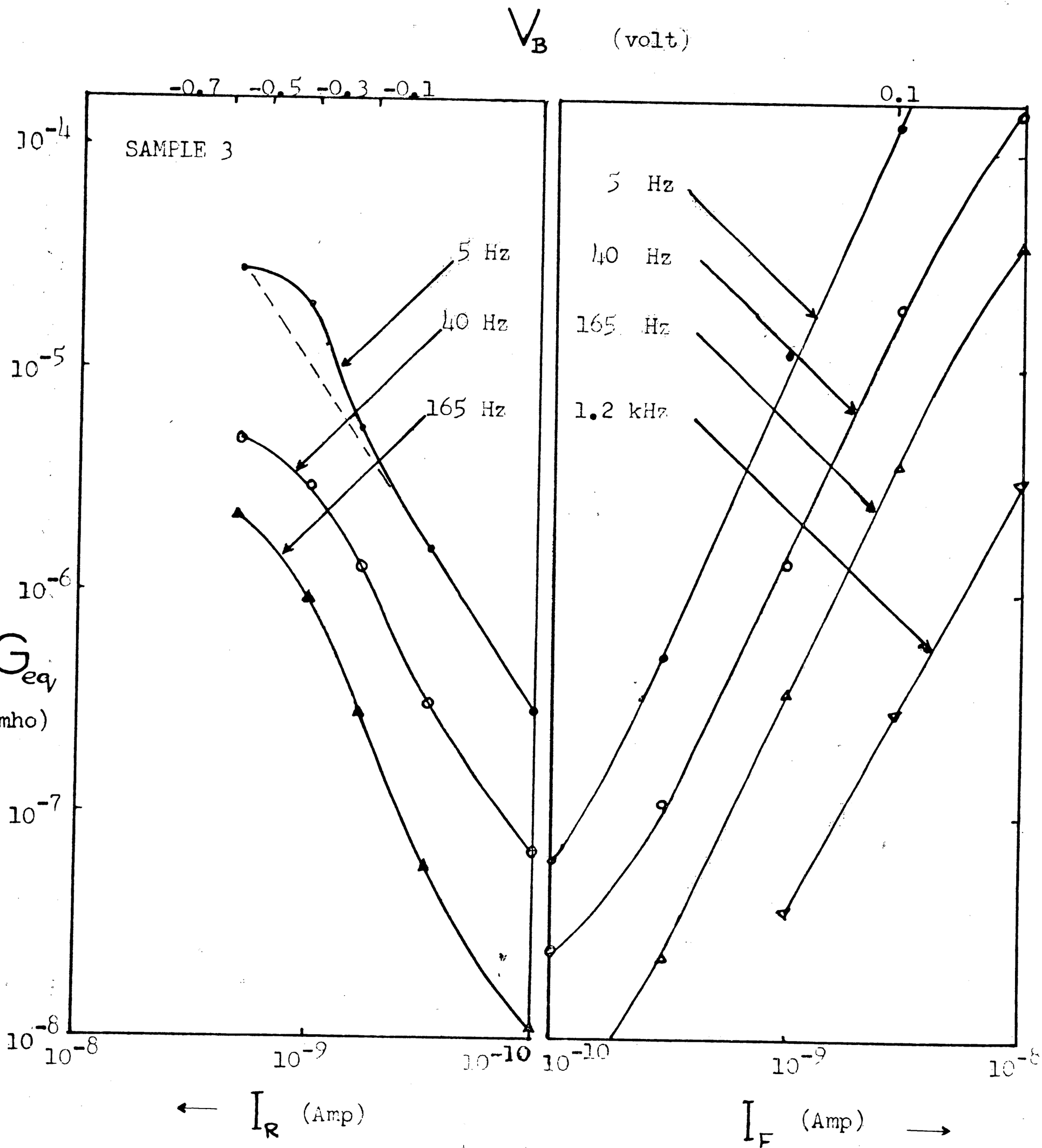


Fig. 20. Measured equivalent noise conductance, $G_{eq}$, vs. bias of Sample 2.

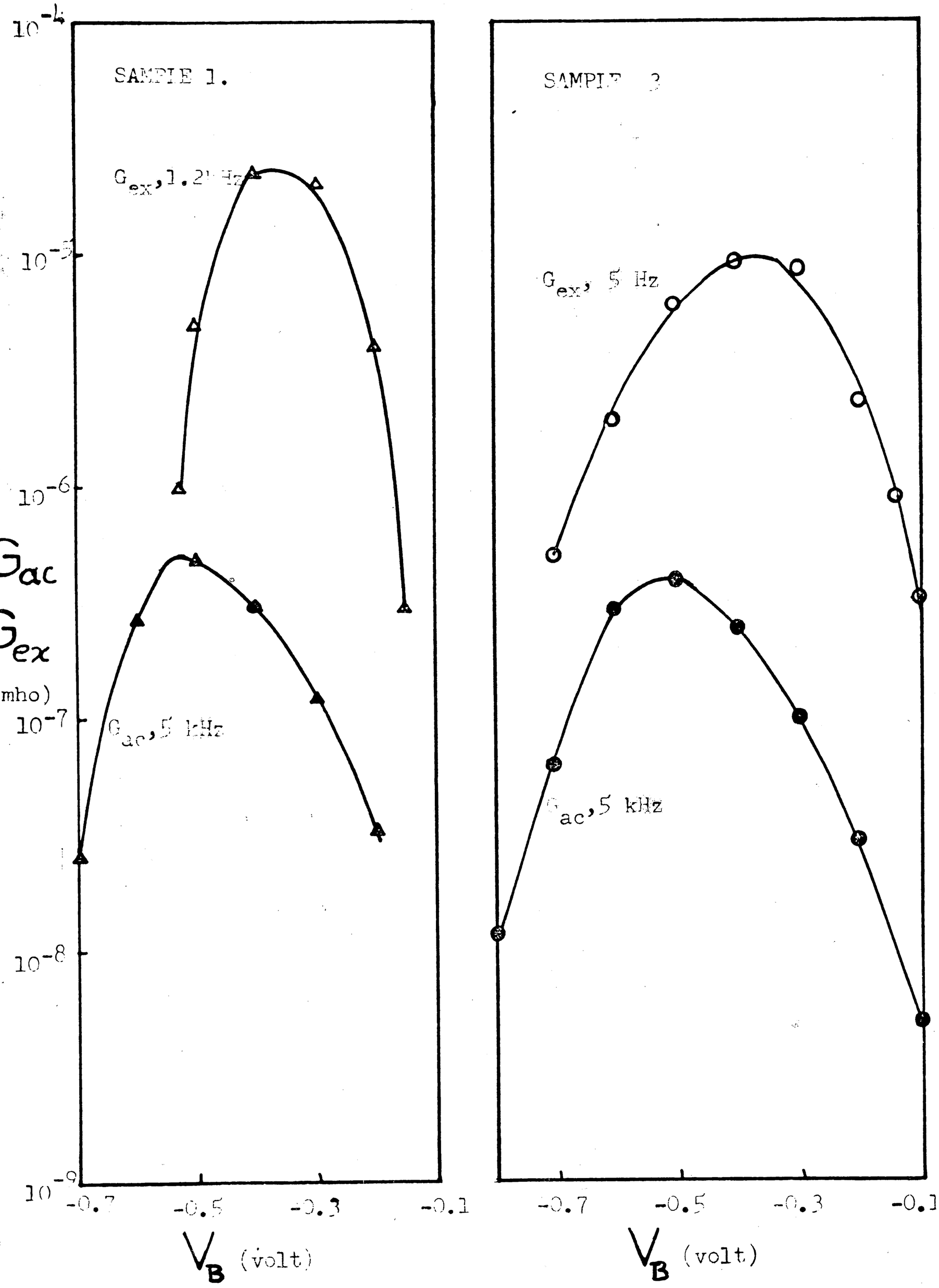


Fig. 21. Ac conductance, $G_{ac}$, and excess noise conductance, $G_{ex}$, vs. bias of Samples 1 and 3.

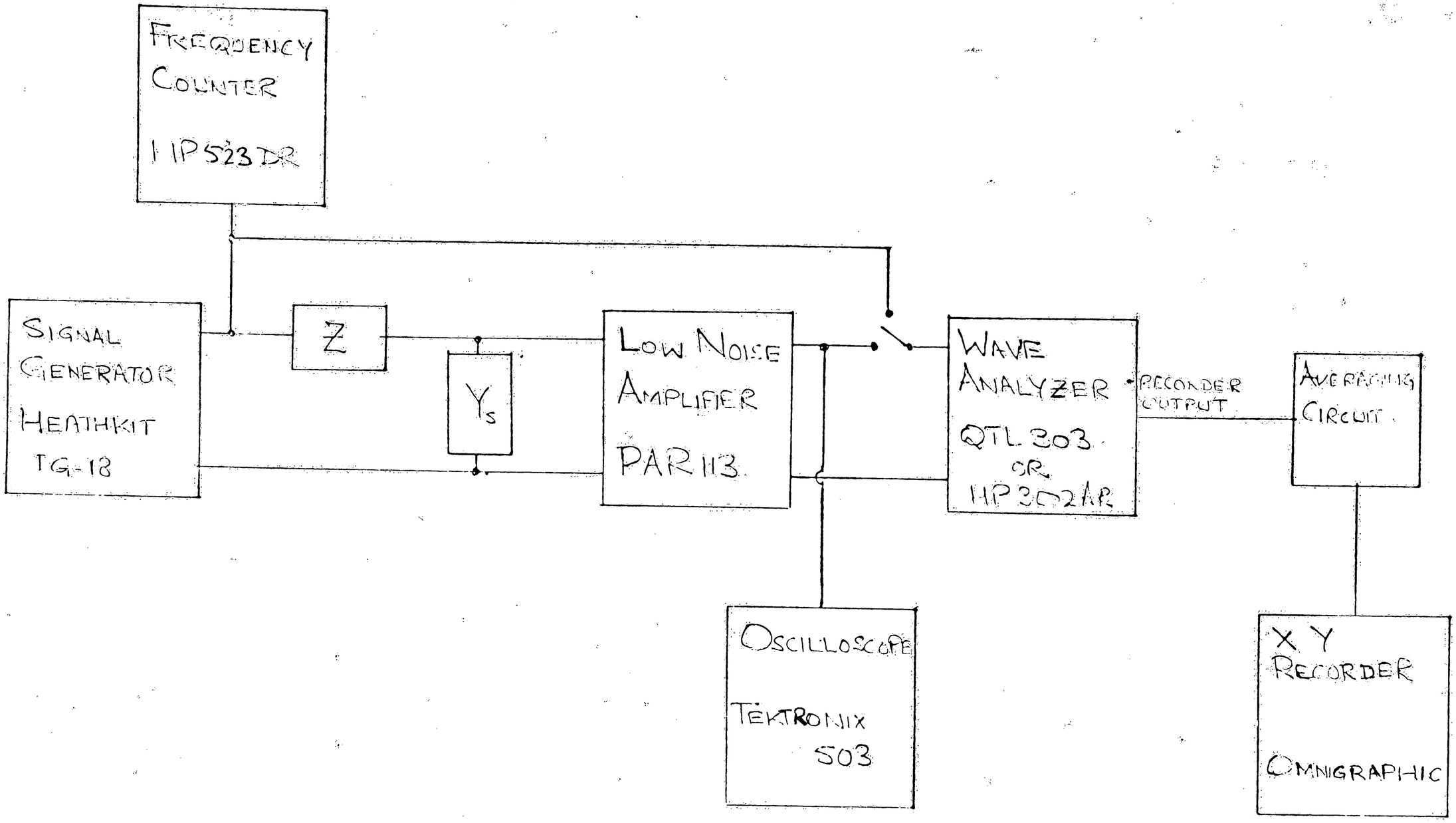


Fig. 22. Set-up used to measure effective noise bandwidth, B, and amplifier noise figure, NF, using signal current source standard.

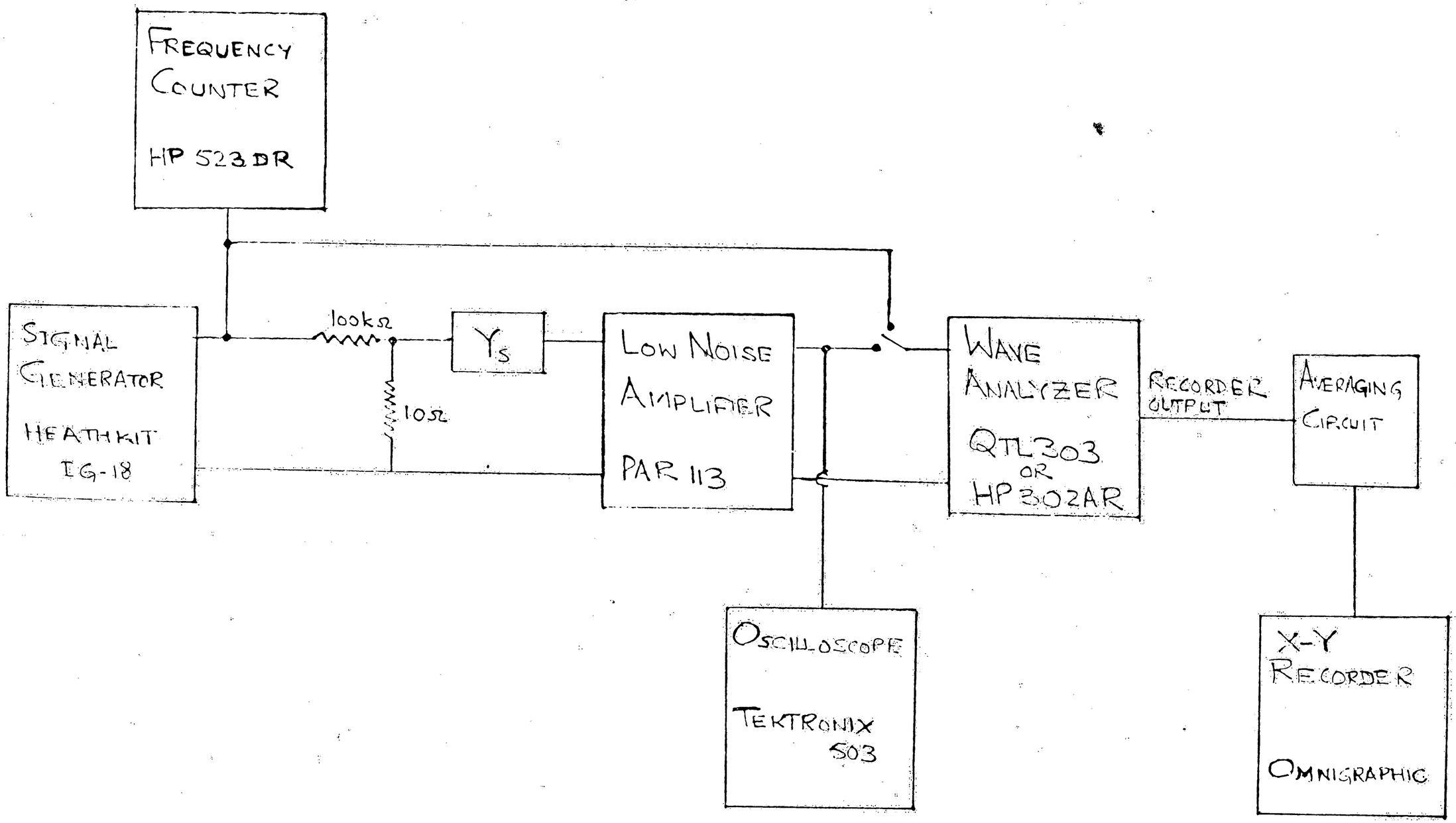


Fig. 23. Set-up used to measure amplifier gain, $A_V$, and amplifier noise figure,,NF, using signal voltage source standard.

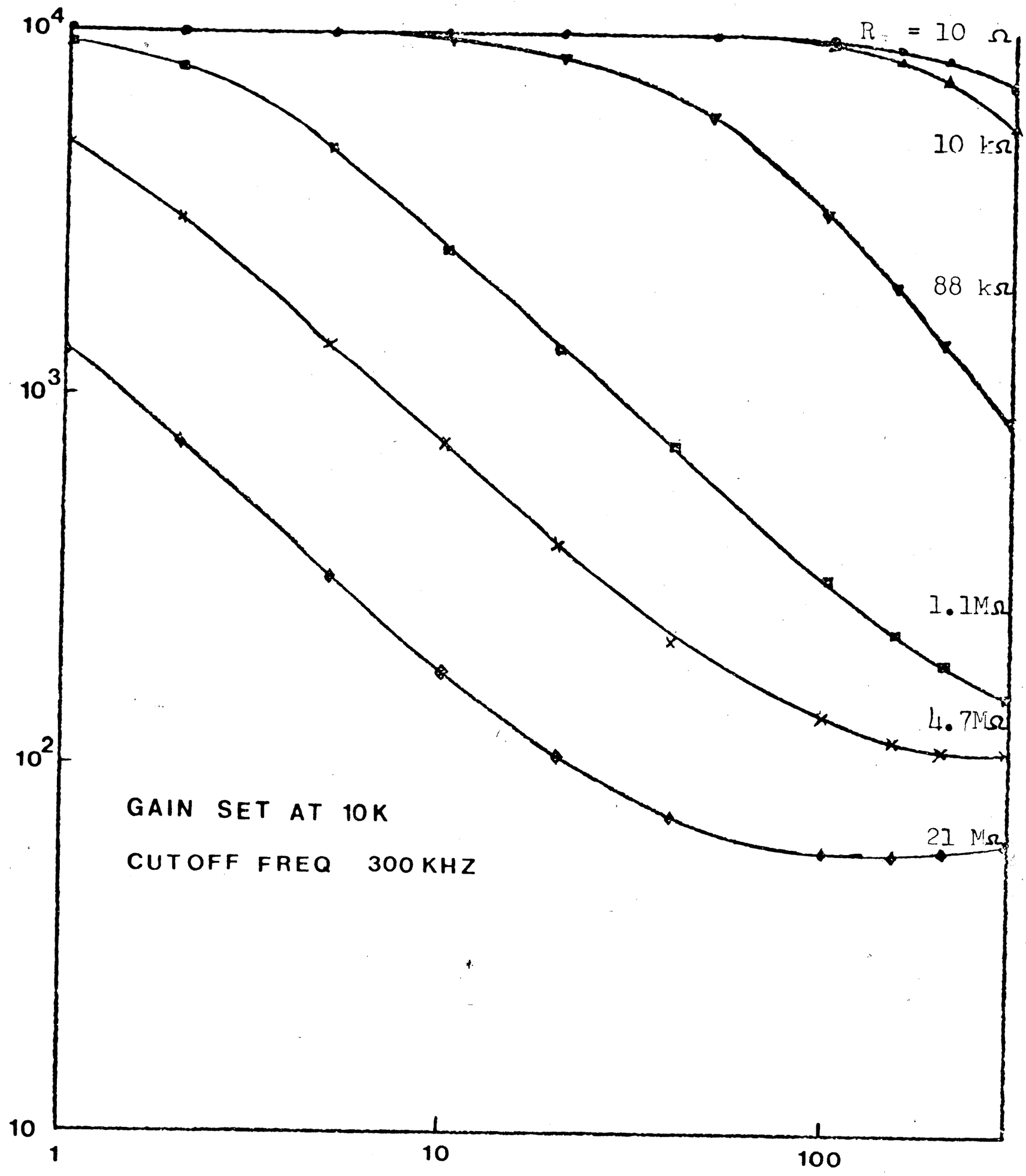


Fig. 24 Measured gain, $A_v$, vs. frequency characteristic with source resistance as parameter for amplifier PAR 113.

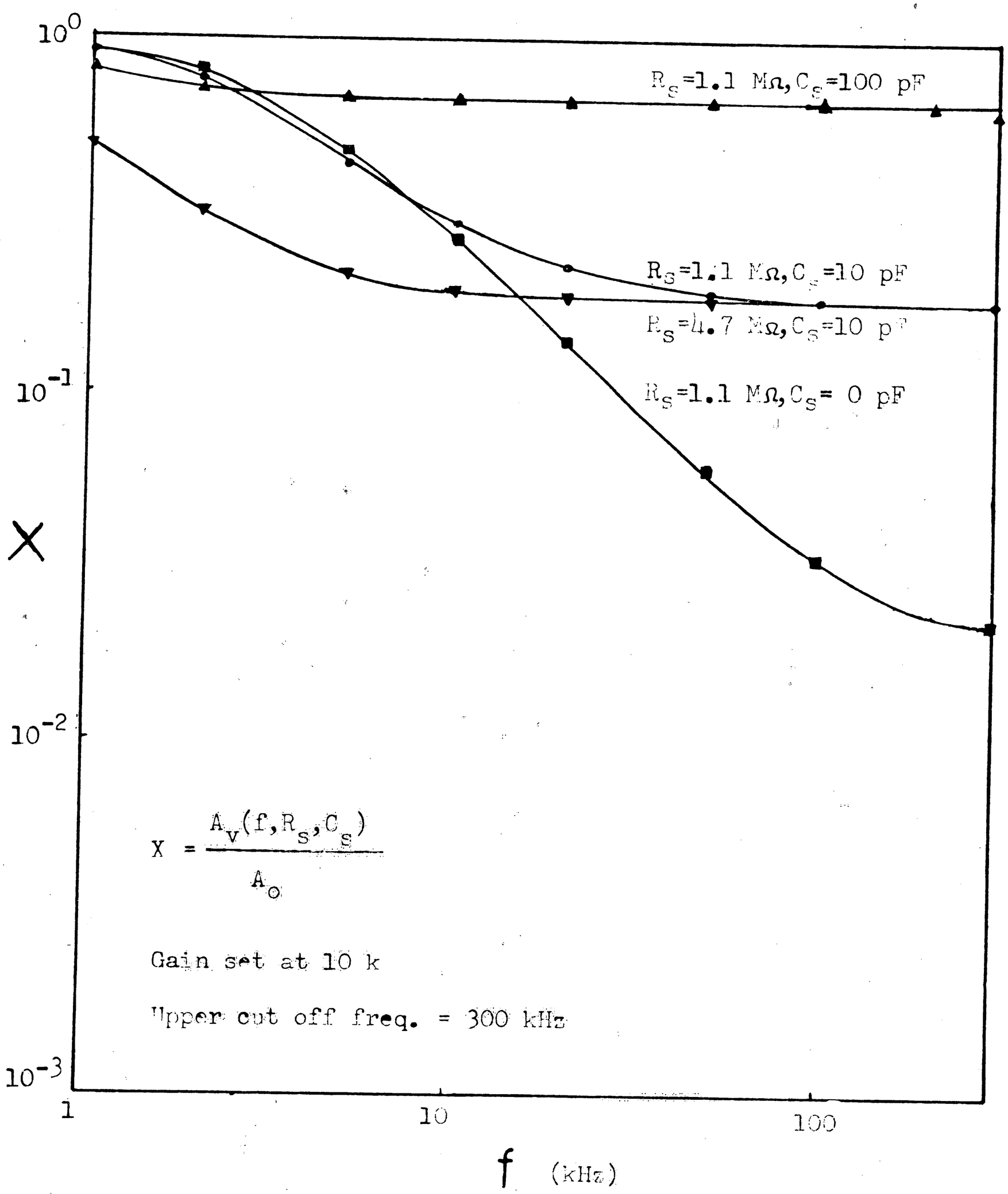


Fig. 25 Normalized gain vs. frequency measured with source impedance as parameter for amplifier PAR 113.

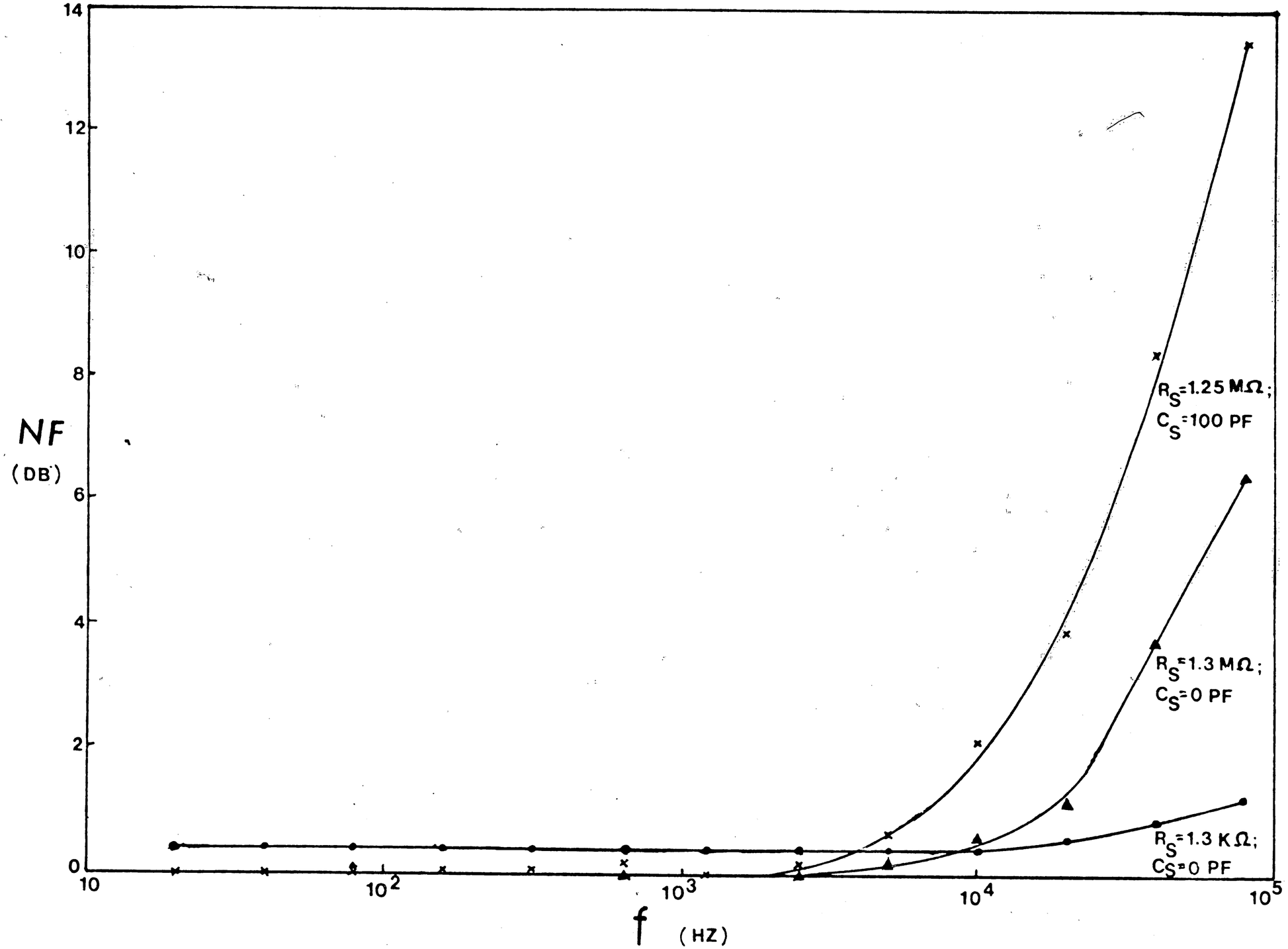


Fig. 26a. Measured noise figure vs. frequency of amplifier PAR 113 using current standard.

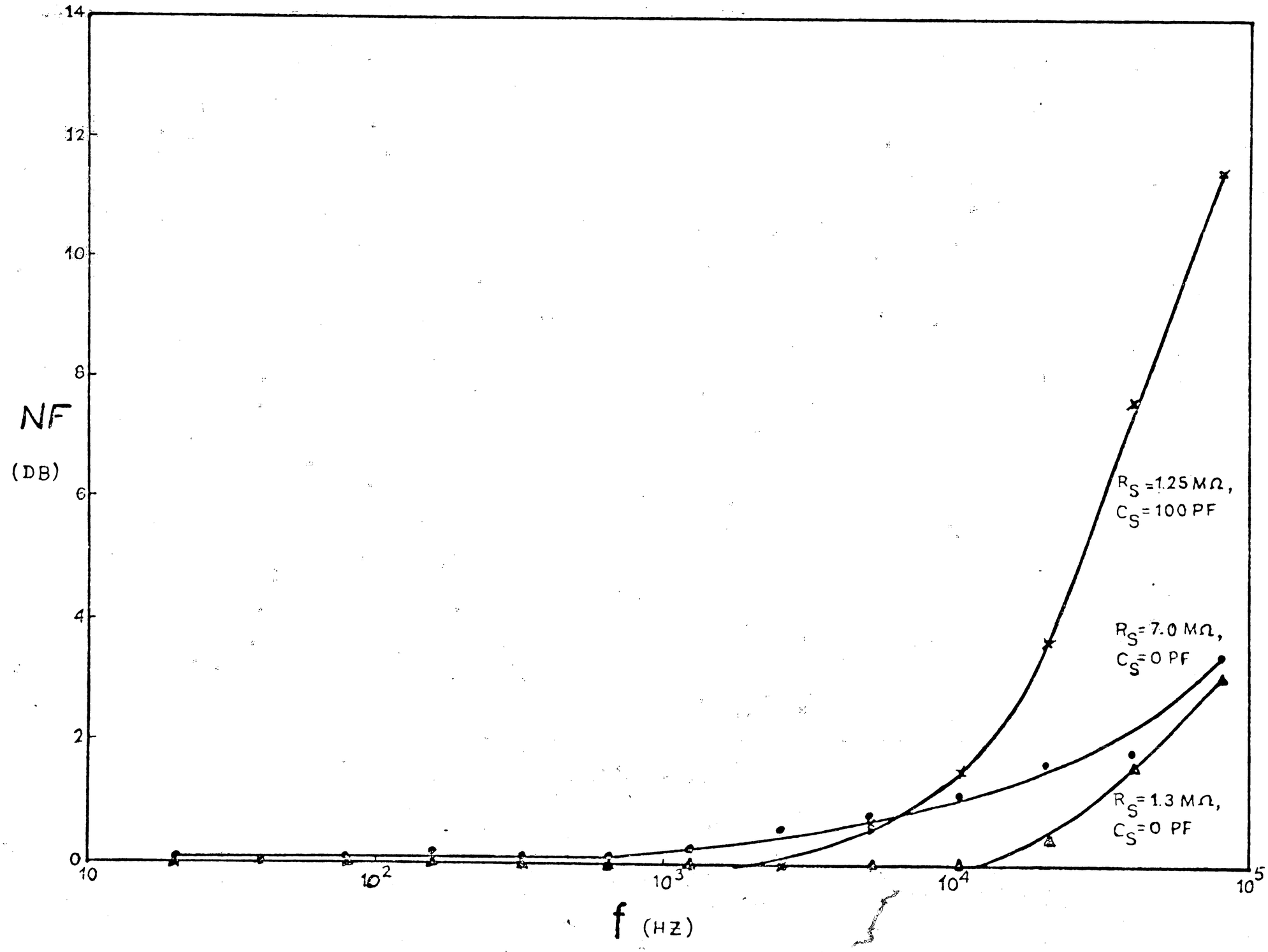


Fig. 26b. Measured noise figure vs. frequency of amplifier PAR 113 using voltage standard.

VITA

Vikram Kumar was born on July 8, 1947, in Lucknow, India. He attended the University of Allahabad earning the degrees of Bachelor of Science in 1965, and Master of Science in Physics in 1967. He enrolled in the Graduate School at Lehigh University in September of 1968 where he is working towards a Ph.D. in Electrical Engineering. He is a member of Eta Kappa Nu and IEEE.